5-2024

Improved Ballistic Impact Resistance of Nanofibrillar Cellulose Films With Discontinuous Fibrous Bouligand Architecture

Colby Caviness
cdcavin@clemson.edu

IMPROVED BALLISTIC IMPACT RESISTANCE OF NANOFIBRILLAR CELLULOSE FILMS WITH DISCONTINUOUS FIBROUS BOULIGAND ARCHITECTURE

A Thesis
Presented to
the Graduate School of
Clemson University

In Partial Fulfillment
of the Requirements for the Degree
Master of Science
Mechanical Engineering

---

by
Colby Dylan Caviness
May 2024

Submitted to:
Dr. Zhaoxu Meng, Committee Chair
Dr. Zhen Li
Dr. Xin Zhao

ABSTRACT

Natural protective materials offer unparalleled solutions for impact-resistant material designs that are simultaneously lightweight, strong, and tough. Particularly, the dactyl club of mantis shrimp features chitin nanofibrils organized in a Bouligand structure, which has been shown to effectively dissipate the high impact energy during powerful strikes. The mollusk shells also achieve excellent mechanical strength, toughness, and impact resistance with a staggered, layer-by-layer structure. Previous studies have shown that hybrid designs, by combining different bioinspired microstructures, can lead to enhanced mechanical strength and energy dissipation capabilities. Nevertheless, it remains unknown whether combining Bouligand and staggered structures in nanofibrillar cellulose (NFC) films, forming a discontinuous fibrous Bouligand (DFB) architecture, can achieve enhanced impact resistance under localized ballistic impact.

Additionally, the failure mechanisms under such dynamic loading conditions have been minimally understood. In this thesis, I present a comprehensive study on investigate the dynamic failure mechanisms and quantify the impact resistance of NFC thin films with DFB architecture by leveraging previously developed coarse-grained models and explicit projectile impact molecular dynamics simulations. The results show that when nanofibrils achieve a critical length with the DFB architecture, the impact resistance of NFC films outperforms the counterpart films with continuous fibrils by comparing their specific ballistic limit velocities and penetration energies. I also look into the underlying mechanisms contributing to this improvement in impact resistance, which include

enhanced fibril sliding initiated at the discontinuous sites, intralayer and interlayer crack bridging, and crack twisting mechanism in the thickness direction enabled by the DFB architecture. Overall, the results in this thesis show that by combining Bouligand and staggered structures in NFC films, their potential for protective applications can be further improved. The findings presented in this thesis can provide practical guidelines for the design of protective films made of nanofibrils.

DEDICATION

I dedicate this thesis to my consistently supportive friends, teammates, and family, my father, Michael Caviness, my mother, Renee Caviness, and my sister, Amber Caviness. I am grateful for everything they have instilled in me and forever thankful for the love they have shown. This thesis would not be possible without the expertise from my advisor, Dr. Zhaoxu Meng and without the support of everyone important in my life.

ACKNOWLEDGMENTS

I would like to thank and acknowledge Dr. Zhaoxu Meng, my advisor and Committee Chair, for his continued guidance throughout my graduate studies and for leading the way into the computational materials science research area. His experience and guidance have been invaluable throughout this research experience. I would also like to acknowledge Dr. Zhen Li and Dr. Xin Zhao for their guidance and feedback in the development of my thesis as committee members. Additionally, I would like to acknowledge Jane Breslin and Cho-Chun (Jonathan) Chiang for their initial work on the mechanical properties of Bouligand microstructures with integrated defects, as well as for being a source of knowledge when I had questions. I would like to thank my mother, father, and sister for being great examples, for their support, and for constantly pushing me to be the best I can be. I would also like to thank my grandmother Joyce Perkins for teaching me the value of education, as well as my friends and family, who have helped me in countless ways throughout this process and in life.

I would like to acknowledge the Graduate Research Fellowship from NASA SC Space Grant Consortium (521383-GRF-CM007). Without the generous funding of this fellowship, I would not have been able to complete my graduate degree as well as travel to multiple conferences to present and listen to some of the brightest minds in the country. This fellowship also allowed me to gain valuable volunteer experience through various outreach programs and share my love of science/engineering with the next generation of engineers. The fellowship experience has changed the trajectory of my career and opened so many opportunities that I would have never been able to without

their assistance. Again, I cannot acknowledge and thank NASA SC Space Grant enough for believing in me and giving me this wonderful opportunity and gift.

I would also like to acknowledge other funding support from SC TRIMH (P20GM121342) the NSF SC EPSCoR Program under NSF Award # OIA-1655740 and SC EPSCoR Grant #23-GE03 and #22-SA01. Clemson University is acknowledged for the generous allotment of computational time on the Palmetto cluster.

TABLE OF CONTENTS

LIST OF TABLES

LIST OF FIGURES

CHAPTER ONE

INTRODUCTION TO CELLULOSE NANOCRYSTALS

Cellulose, one of the most abundant biopolymers on Earth, which embodies roughly 50% of all dry mass plant structural material as well as found in organisms including bacteria, algae, and tunicates [1-7]. It is the primary structural component of plant cell walls and serves as a vital source of renewable and sustainable materials. As the need for safe, renewable, and biodegradable materials urgently increases, cellulose materials and nanocomposites have exploded in research prevalence as we try to solve some of the biggest issues facing our world today, including resource consumption, health, and environmental impact. Cellulose has drawn the attention of so many in research, not only because of the promising renewability and biodegradability factors but also because of the seemingly inexhaustible resource that can be found all over the world [8-10]. Figure 1 shows the hierarchal structure of cellulose found in nature, particularly in wood from trees. Specifically, cellulose is composed of a linear chain with repeat units of two anhydroglucose rings. Rich hydrogen bonds between adjacent cellulose chains promote parallel packing of cellulose chains into sheets (Figure 1(a)), which are further stacked together by van der Waals forces into elementary fibrils, also known as nanofibrilated/nanofibrillar cellulose (NFC) or cellulose nanofibers/nanofibrils (CNFs). NFCs are constituted of ordered crystalline regions along with disordered (paracrystalline and amorphous) regions and the nanoscale crystalline regions are termed as cellulose nanocrystals (CNCs). At the even larger hierarchical scales, NFCs aggregate and order

themselves across multiple length scales to support structural stability and strength to trees (Figure 1(b)).

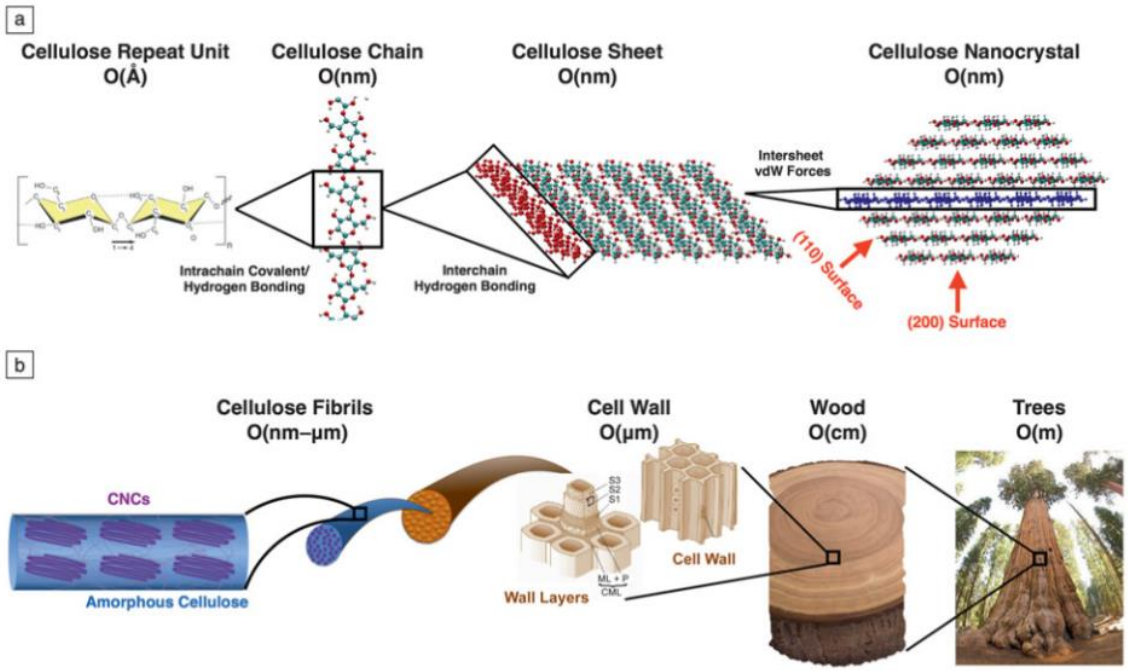

FIGURE 1: Hierarchical structure of CNCs in wood/trees. (a) Schematic illustrating the formation of CNCs from repeat units. Multiple cellulose repeat units are linked together by covalent bonds and intra-chain hydrogen bonding into cellulose chains. These cellulose chains form sheets by extensive inter-chain hydrogen bonding. CNCs are stabilized into multiple cellulose sheets via van der Waals forces. (b) Hierarchical structure of cellulose in trees. Cellulose fibrils consist of CNCs embedded in amorphous cellulose domains. These fibrils aggregate and order themselves across different length scales to wood cell walls to offer structural stability and strength to trees. Adapted from Sinko et al. *MRS Bulletin* 2015 [2].

The nanoscale cellulose materials exhibit exceptional properties such as high aspect ratio, self-assembly capability, tunable surface chemistry, and biocompatibility. Such cellulose nanomaterials can be extracted using different methods from woody materials and show great promise in enhancing mechanical properties of composites/nanocomposites as reinforcements while being more environmentally friendly. This introductory chapter

delves into the history and applications of cellulose nanomaterials with a focus on CNCs, shedding light on their emergence as a cutting-edge material with a vast range of uses.

1.1 Historical Perspective

First discovered in 1838 by Payen [11], Cellulose, a linear biopolymer composed of repeating anhydroglucose units ($(C_6H_{12}O_5)_n$) where *n* can range from a few hundred for wood pulp to tens of thousands based on source material) connected by a large fraction of 1β crystal structure (68-94%),4-glycosidic bonds, is a complex, hierarchical material. Its inherent strength, abundance, and biodegradability made it an ideal candidate for novel applications. Early research focused on breaking down cellulose into nanoscale dimensions, giving birth to CNCs. The history of CNCs can be traced back to 1947 when scientists began to recognize the unique properties of cellulose at the nanoscale [12]. These particles have also been named nanocrystalline cellulose, cellulose whiskers, cellulose nano-whiskers, and cellulose microcrystals according to the early literature. CNCs are rod-shaped (whisker-shaped) particles that are remaining after acid-hydrolysis of most cellulose particle types. These nanocrystals have a crystalline core with dimensions on the order of several nanometers, making them unique and promising materials. CNC's with their high aspect ratio with 100% cellulose and have a high natural crystallinity (on the order of 54-88%) [13].

1.2 Extraction and Properties

Cellulose has a natural tendency to have regions of high crystalized structure as well as amorphous structures. CNCs are typically extracted from cellulose-rich sources, such as wood pulp, cotton, or agricultural residues, through a combination of mechanical,

chemical, or enzymatic processes. The most common extraction method for CNCs involves acid hydrolysis of general cellulose concentrated sulfuric acid which gives to rise to the highly crystalized rod-shaped nanofibers [14]. The resulting nanocrystals possess exceptional properties, including high mechanical strength, low density, and exceptional thermal and optical characteristics. There has been a wide range of cellulose sources that can be utilized to isolate the nanocrystals such as wood pulp, cotton, ramie, rice, microcrystalline cellulose (MCC), bacterial cellulose and more [15-26]. Their colloidal nature and high surface area have also made them attractive for a wide range of applications, spanning various industries. Figure 2 below, shows how CNCs can be manufactured. In (A), there is an extracted cellulose region that has crystalline and amorphous regions, then through sulfuric acid hydrolysis the amorphous region can be dissolved out leaving the crystalline regions which are known as CNCs. In (B), we can see TEM micrographs of CNCs after the amorphous region is dissolved out of various cellulose sources.

The schematic of potential manufacturing processes to create cellulose nanocrystals shows the relative ease and wide sources that can be utilized. This process has significant potential to be scaled to high volume manufacturing to address the material shortages that have been seen since the pandemic [27], and shows how conditions within the solvent can affect the hierarchal structure and properties of the CNCs.

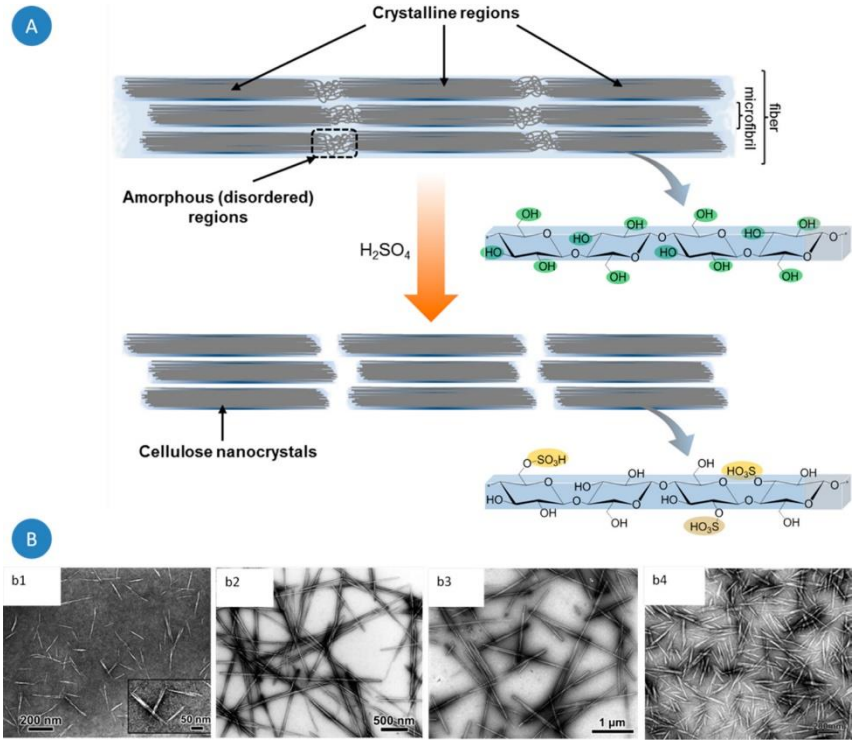

FIGURE 2: Schematic of idealized cellulose nanofibers. (A) Shows one of the suggested configurations of the crystalline and amorphous regions, and CNCs after sulfuric acid hydrolysis of the disordered regions, exhibiting the characteristic sulfate half ester surface groups formed as a side reaction. (B) TEM micrographs of dispersion of CNCs derived from different sources: (b1) microcrystalline cellulose (Avicel), (b2) tunicate,(23) (b3) green algae (*Cladophora sp*.),(18) and (b4) ramie. Reprinted from Domingues et al. *Biomacromolecules* 2014 [14].

CNCs have garner significant attention in the advancement of material science due their miniscule dimensionality (2-50 nm width by 100-2000 nm length) [28] conversely compared to their excellent material properties when axial loaded the longitudinal modulus can range from 110 to 220 GPa and tensile load baring between 7.7-7.9 GPa [1, 29]. Similar to CNCs, NFC, the elementary fibrils in the wood and plant biosynthesis process that consists of 36 cellulose chains, has also been utilized to help gain valuable knowledge about nanocellulose since they are both nanoscale cellulose fibers that have proven reinforcement effects in polymer nanocomposites [6].

Particularly, NFC is a promising building block to replicate the Bouligand and brick-and-mortar structures found in biomaterials at nanometer length scale [30-36].

NFCs are generally more entangled long nanofibrils of cellulose in its structure compared to CNCs and has slightly different mechanical properties due to the presence of amorphous regions [37]. In this thesis, however, CNCs and NFCs are both considered long strand cellulose nanofibrils and we use them interchangeably with an emphasis for simulations conducted on NFCs.

1.3 Applications of CNCs/NFCs

Through chemical modification of CNCs or NFCs, a vast panoply of potential modifications can be unleashed which makes them ideal candidates as a reinforcement nanofiller material and opens the door to countless other applications [9, 38]. The versatility of such cellulose-based nanomaterials has led to their adoption in diverse applications, spanning from traditional industries to cutting-edge technologies. Some of the key domains where cellulose nanocrystals have found applications include:

Materials Science and Engineering:

- Reinforcement in polymer composites to enhance mechanical properties.
- Development of transparent and flexible films for electronic devices.
- Fabrication of biodegradable and sustainable packaging materials [39].

Biomedicine:

- Drug delivery systems with controlled release properties.

- Tissue engineering and regenerative medicine applications. Bio-implants with cellulose nanocrystals coatings have been utilized to limit the corrosion of the implant [40].
- Wound dressings and biocompatible coatings for medical devices.

Environmental and Sustainability:

- Water purification and filtration systems.
- Sustainable nanocellulose-based materials for construction.
- Biodegradable nanopapers and sustainable inks [41, 42].

Energy and Electronics [43]**:**

- Electrode materials for energy storage devices.
- Transparent conductive films for solar cells and touchscreens.
- Dielectric materials for electronic components.

1.4 Future Perspectives

The field of cellulose nanomaterials is rapidly evolving, and ongoing research continues to expand their applications and optimize their production methods. As research has shown the promise of NFCs materials, production of all-cellulose materials has begun as the next step to cultivate applications of them. Currently, solution casting techniques of suspended NFC use evaporation, vacuum filtration, and novel pressing, all of which have proven desirable and impressing adjustability of material properties such as density, porosity, and nanoscale structures [42, 44, 45]. One particular state-of-art technique in fabrication uses cold drawing (shear-based) film casting [46] leading to crazing of the uniform distribution of CNCs. As will be discussed more later, the purpose

of this research is to understand how defects or discontinuous Bouligand fibers will react to impact, and this manufacturing process will allow us to create these discontinuities within the film and eventually will be able to precisely control defect distributions in the material. This is a promising manufacturing technique for this specific research and material structure to advance material modulus and strength. Furthermore, it has been shown that biomimetic designed high-performance materials with brick-and-mortar structure induces a collegial enhancement of stiffness, strength, and work-to-fracture ratio of CNC nanopaper fiber alignment through wet-drawing [47]. These mechanical properties are what has made NFC such a large research topic due to the abilities and applications these material promise.

This thesis aims to explore the history and the latest research on Bouligand structured films consisting of CNCs/NFCs, providing an in-depth understanding of their potential in impact-resistant materials. In the following chapters, we will shed light on their role in shaping a more sustainable and materially advanced world by optimizing bio-inspired micro-architectures using NFCs.

CHAPTER TWO

INTRODUCTION TO BOULIGAND MICROSTRUCTURES

Architected materials from nature with excellent mechanical and protective properties inspire the development of impact-resistant and lightweight synthetic materials [48-51]. The Bouligand structure is commonly found in structural design in nature that involves uniaxially arranged fibers/fibrils in a helicoidal form, with each layer rotating at a certain pitch angle (γ) from adjacent layers as shown in Figure 3 below. This architecture can be widely found in fish scales, crustacean exoskeletons, bones, and many more natural materials, each with unique mechanical properties that cater to the specific functions necessary for the organism's survival [50-52].

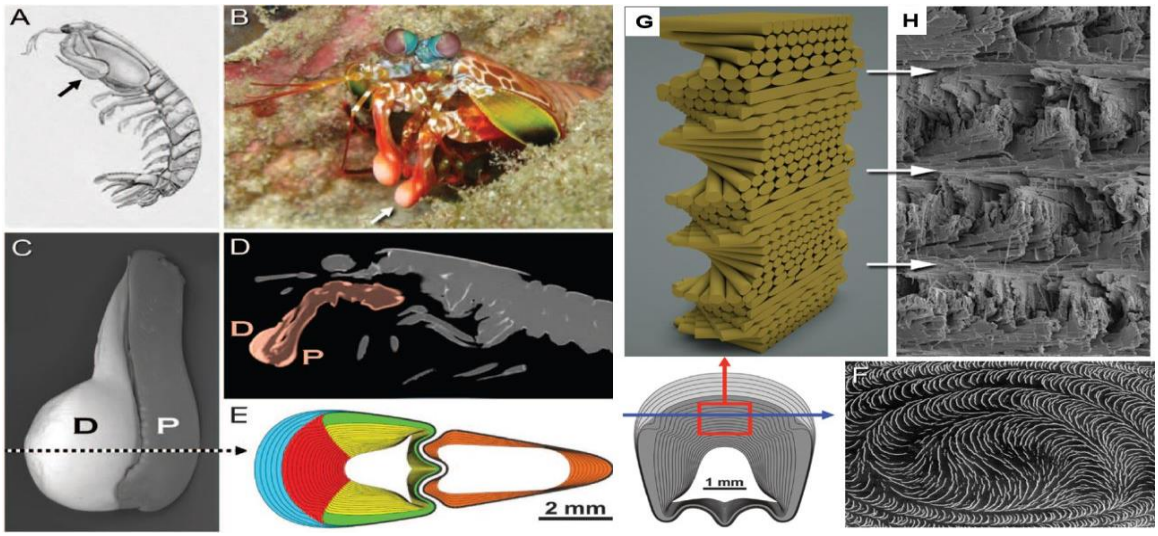

FIGURE 3: Show of morphological features and helicoidal structure of the stomatopod dactyl club. (A-E) A generalized stomatopod body plan and magnified view of impact region on club as well as different constituent dactyl (D) and porous (P) segments. (F) Charged contrast scanning electron micrograph of damaged coronal cross section. (G-H) Comparison between generalized 3D model of helicoidal and SEM fractography. Adapted from Weaver *et al.*, *Science* 2012. [53]

There are four key principals for nature inspiration as defined by Wang et. al, they are as follows: Foundation, Nature Inspiration (self-assembly, hierarchy, function integration), Functionality Design, and Efficiency and Sustainability [54].

Foundation is the synergistic triangle between structure, functionality, and manufacturing. Structure can affect the functionality and manufacturing process; similarly, manufacturing process can alter the structure and functionality of the material. Then to finish this synergistic relationship, the desired functionality guides material selection (structure) and manufacturing process required. Natural inspiration is using well known natural system to help direct and facilitate the direction of material advancement. Many natural systems organize themselves into complex architectures without external stimuli, hierarchical organization gives rise to the advancement of functionality on multiple scales [55]. This key principal is essentially mimicking naturally occurring phenomena into our material development to give them these special abilities to achieve greater function integration[56]. Functionality design is understanding how the dynamic evolution over billions of years have created these sophisticated sensing mechanisms, responsive and optimized structures found in nature; which can then be effectively used to advance materials that are sensing, adaptive, and responsive [54]. The final key principle is efficiency and sustainability as nature has shown to be highly efficient. Learning from their efficiency, more sustainable and eco-friendly solutions can be developed resulting in a decreased environmental impact as we continue to advance.

Another important attribute that fascinates researchers is the millions of years of evolution that natural materials must go through to have survived. Through this

evolution, these novel materials have perfected their structure, property, and function as remarkable solutions to many of our current real-world problems; that we as a society have not been able to overcome without assistance from bio-inspired materials. Bio-inspired materials and systems are constantly in new development to be utilized to solve technical challenges in architecture, engineering, chemistry, biomedical, and material science [57, 58]. Nature-based nanomaterials possess intriguing properties including extraordinary mechanical performance, adaptive surfaces, and hierarchical assembly to be potentially employed for novel structural and functional macroscopic materials [59-61].

2.1 Bio-Inspired Studies

As previously discussed, billions of years of evolution has created novel solutions to untapped problems that are now being analyzed in a new field of bio-inspired studies. Bio-inspired materials have led to a wide range of new questions and research topics, none more puzzling than how a material can be tailored to achieve desired compromise between different functions. In the case of transient structured bio-inspired materials, continuous tissues must have a transition between mineralized skeletal elements (bone) and arthrodial membranes (tendon) which is of particular interest since the mechanical properties can drastically between structures.

To get such a wide range of material properties in a single material requires a high degree of freedom in structural and compositional organization; an example of this would be the tendon-to-bone interface. This tendon-to-bone interface is fascinating to try understanding the mechanisms within and how to model this phenomenon which has

been thoroughly researched with promising results [62-70]. The tendon-to-bone interface is one of many current bio-inspired studies, others include: virus-mimicking drug delivery [71], natural material toughening strategies to more sustainable structures [72], chameleon inspired cellular force imaging with photonic crystals [73], and even engineered living materials for more sustainable and resilient architecture [74].

From a study on the fish scales of *Arapaima gigas*, one of the largest freshwater fish in the world, it was found that the scale has an inner layer that consists of mineralized collagen fibrils in a Bouligand structure. It helps minimize penetration damage from predators through various toughening mechanisms, such as crack twisting and fibril bridging [49, 75, 76]. In addition, the material's natural flexibility also assists in the energy redistribution of compressive stresses [50]. Similarly, the dactyl clubs of stomatopods, e.g., mantis shrimp, can withstand immense stress from strong impact strikes against their prey, most often protected by mollusk shells. The dactyl club is composed of mineralized chitin nanofibrils organized in a Bouligand structure. The fact that the dactyl club can easily crack the mollusk shells demonstrates the excellent impact resistance of the Bouligand structure.

Recently, the Bouligand structure has led to impact-resistant materials design concepts that show promising applications in automobiles and body armor [77-81]. On the other hand, during the survival war between predators and prey, the mollusk shells also evolve excellent mechanical and protective properties that simultaneously achieve high mechanical strength and toughness as well as impact resistance [82-88]. Particularly, the inner layer of the mollusk shell, known as nacre, composes of nano-sized mineral

platelets and a biopolymer matrix in a brick-and-mortar type of staggered arrangement. Nacre possesses excellent fracture toughness that is orders of magnitude tougher than the constituents and has been widely regarded as one of the best natural body armors due to its unique multiscale architectures [1, 30, 89-92].

It is generally understood that the hierarchical organization within the cuticle is based on the structural polysaccharide molecule chitin and its composite nature [93]. Recent studies have shown the classical hierarchy of the organic matrix is regularly varied in functional adaptability as well as structural arrangement and composition in individual levels [94-101]. The hierarchal nanostructure of different species and how they become organized in helical (Bouligand) stacks is shown in Figure 4 below.

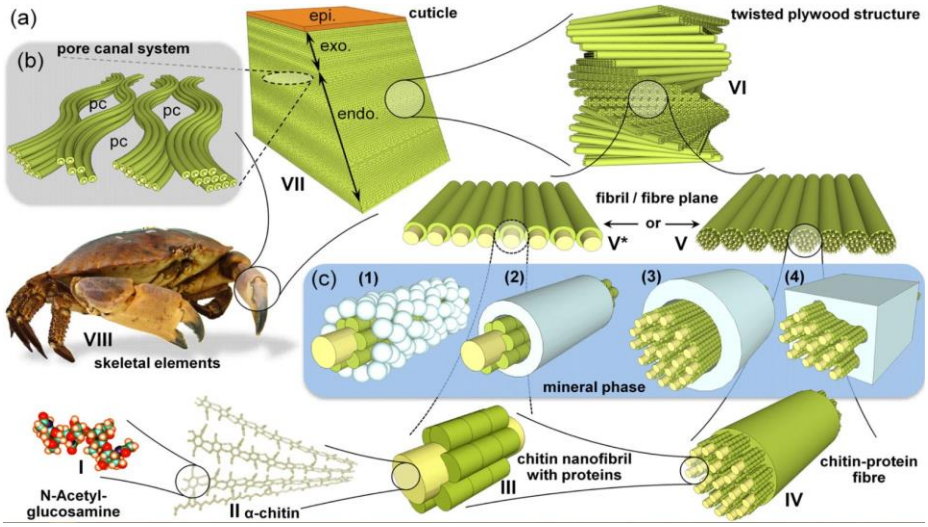

FIGURE 4: Structural hierarchy of cuticle forming skeletal elements with different functions in different Crustacea species. (a) Organic matrix: N-acetylglucosamine molecules (I) form anti-parallel chains of α-chitin (II). Protein-coated chitin crystallites form nanofibrils (III) that can either form horizontal planes (V*) or assemble to chitin protein fibers (IV) arranged in horizontal planes. (V). Helicoidally stacked planes of nanofibrils or chitin-protein-fibers forming the twisted plywood structure (VI) constituting the procuticle. Together with the outermost epicuticle, the procuticle (VII) forms different skeletal elements (VIII). (b) The pore canal system pervades the procuticle in normal direction. Depending on species and function of the skeletal element, the canals can vary in numbers and have different shapes, sizes and structural

modifications. (c) Structural modifications of the mineral phase observed in different species and skeletal elements. Nanofibrils can be decorated with spherical particles (1) or enclosed by mineral tubes (2), which was also observed for larger chitin-protein fibers (3). In some cases, clusters of nanofibrils occur embedded in a solid mineral matrix (4). Reprinted from Fabritius *et al*., *Bioinspir. Biomim*. 2016. [102]

The encouraging results from bio-inspired material research has created revolutionary materials that are much more capable and configurable than current materials [31, 52, 54, 74, 85, 103-114]. As manufacturing has advanced so has the materials being produced and with the further development of bio-inspired materials the research conducted has become be applicable to solving the problems we face today. While the advancement of bio-inspired materials continually grows, more research has been conducted on Bouligand architecture for enhancement in mechanical properties and concurrently developing manufacturing processes.

2.2 Bouligand Manufacturing Processes

Given the excellent performance of such biomaterials with unique structures, tremendous efforts have been devoted to fabricating biomimetic materials by replicating or resembling the unique structures of biomaterials. Previous efforts have applied different fabrication methods to resemble the Bouligand and other bioinspired structures [76, 115-119]. One of them 3D printed specimens with Bouligand structure, but they showed no improvements in critical failure energy and resisting crack initiation [118]. Another study prepared carbon fiber-reinforced epoxy specimens with a helicoidal layup similar to the Bouligand microstructure [119]. The plies in these specimens were manually cut and laid according to the layup specifications and then cured in an oven. Another common manufacturing process for this type of architecture similarly manually

laying prepreg fibers in a helical pattern with a predetermined pitch angle for each layer, however followed by vacuum sealing/pressing the material compactly, followed by a curing process determined by the fibers and matrix material [120].

As previously discussed, CNCs and NFCs have the tendency to formulate this helical structure and can be tuned by external conditions and treatments. Some important tunable parameters including optical properties [121], concentration [122], and pitch angle between layers.

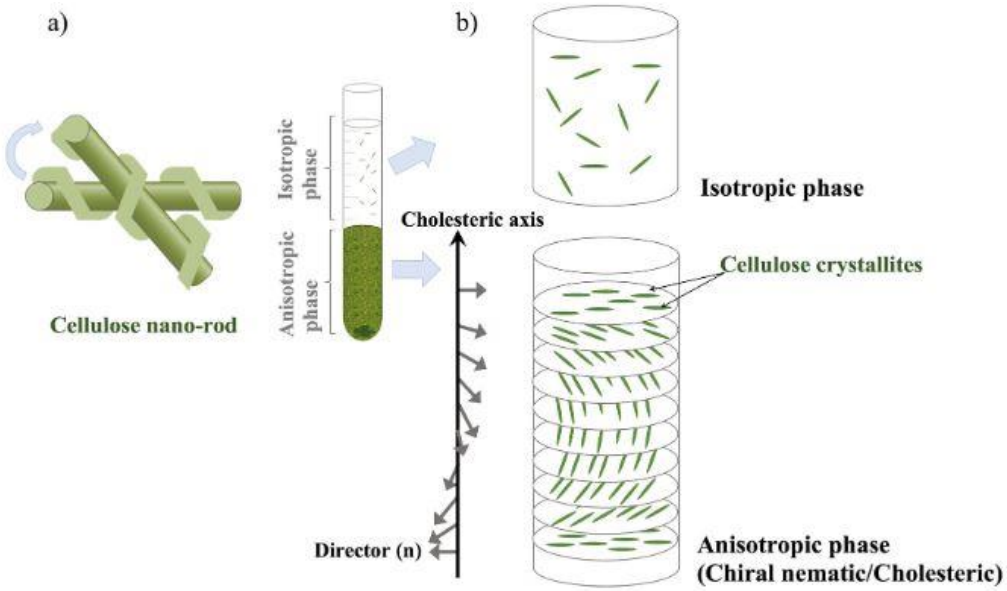

FIGURE 5: Chiral nematic structure of CNCs. (a) helical twist of CNCs and (b) helical twist of CNCs layers along the cholesteric axis. Reprinted from Saffarionpour S, *Food and Bioprocess Technology* 2020. [36, 123, 124]

This self-assembly is a key characteristic of CNCs/NFCs that makes it advantageous for preparing bioinspired structural materials, which are promising for future structural and impact-resistant applications [106, 111, 125-129]. The γ of these self-assembled Bouligand microstructures can be controlled by the conditions within the

water solvent used [128, 130]. This is important to note because γ can be an important design variable for desired functions.

The manufacturing processes of 3D printing and manually laying up in the macroscopic scale to water treating in the microscopic scale show the extensive size capabilities of current manufacturing technologies to create the Bouligand architecture. However, these are labor intensive processes that require significant time and money to fabricate so advancements will need to be made to make this structure more readily available. This is particularly why the research conducted here and by others is crucial to show the viability and possibility of Bouligand architectures to increase the desire to develop more efficient and cost-effective processes for these complicated structures.

2.3 Experimental Studies on Bouligand Structured Films

Experimental transverse testing showed that specimens with lower interplay angles (pitch angles, γ) could sustain higher loadings with a 34% increase in peak loading for 19-ply laminates. Micro-CT scans further show transverse cracking and delamination along the helicoid climb forming a spiral pattern [119]. It is important to note that these aforementioned case studies resemble the Bouligand structure at the macroscopic scale. It shows the scalability of these structures for larger-scale real-world applications. However, it may not be able to leverage the enhanced performance by adopting such structures at similar length scale as those in natural materials and may lead to insufficient mechanical performance compared to natural materials.

In a study conducted by Mencattelli [131], they constructed novel a Herringbone-Bouligand CFRP to further enhance the impact resistance and delamination of classical

Bouligand microstructures. This tuning led to a 13% increase in total dissipated energy, 62% increase in dent diameter before critical failure and significant reduction in delamination area (71%) compared to the classical Bouligand structure we analyze here. This study and countless others show the promise of Bouligand structures integrated with CFRPs to create highly specialized materials that are stronger than current materials [92].

An interesting study was conducted by Yin et. al. that studies the difference between single Bouligand structures that are commonly observed and the rarer double twisted Bouligand structure that can be found in coelacanth fish [132, 133]. Yin observed through the model the critical role played by the extra inter-bundle fibrils found in coelacanth fish scales in enhancing the toughness of Bouligand-type structures with a significant increase in impact resistance. The study verifies these results with synthesis and fracture tests of 3-D printed Bouligand architected materials to support the modeling and understanding of the fracture mechanisms.

As mentioned in the last section, NFC is a particularly promising building block to replicate the Bouligand and brick-and-mortar structures found in biomaterials at nanometer length scale. In addition, NFC has excellent mechanical properties comparable to Kevlar and other nanofibrils [1, 30]. However, achieving the optimal design of such structures utilizing NFCs is a dauting experimental task as a very large number of design parameters can affect the final performance and carrying out experiments on such nanostructured films is very time and cost consuming. In this regard, computational modeling and simulations offer great advantage in much cheaper virtual design and testing, understanding the structure-property relationships, and understanding the

underlying fundamental mechanisms. Additionally, theoretical mechanics will offer great insights in deciphering such relationships and mechanisms.

In the next chapter, I will talk about recent efforts in modeling and simulations of CNCs and NFCs and Bouligand-structured films, with a focus on modeling efforts of the nanocellulose films with Bouligand structures. I will also briefly discuss theoretical mechanics models that can describe the vast inter-fibril mechanics that govern the overall mechanical properties of such films. At the end, I will point out the remaining knowledge gap on the optimal design of Bouligand-structured films made of NFCs, which serves as the motivation for this thesis research.

CHAPTER THREE

PREVIOUS MODELING AND SIMULATION EFFORTS

3.1 MD Simulations and Coarse-Grained Modeling

It thus becomes critical to understand the underlying mechanisms and come up with design principles for structural materials made of NFC with enhanced impact resistance and other mechanical properties. In this regard, computer simulations offer great promise and can save significant time and costs compared to experiments. Particularly, molecular dynamics (MD) simulations are powerful tools to examine structural-property relationships and underlying deformation mechanisms of nanostructured material systems.

MD simulations model the movement of particles based on Newton's Law of Motion, which gives rise to two basic elements: initial positioning of particles and the interactions of particles. All-atomistic (AA) systems follow the exact atomistic structure of the system and has simulated harmonic potential energy between bonds as a spring. Since we are modeling polymer systems, van der Waals interactions with pair-wise potentials will be used. Pair-wise potentials usually model both attractive and repulsive interactions and the potential form we use is known as 12-6 Lennard-Jones potential. With structure and force across the field known, we can obtain the forces exerted on each particle and through integration over time, impact trajectories of the particles can be determined. Through these simulations we can gain valuable information on system

properties and experiment various conditions to further analyze a material without the costly expenses of experimentation.

Furthermore, coarse-grained (CG) modeling techniques have grown in popularity due their ability to significantly increase the potential of computational simulations, while maintaining the accuracy of traditional modeling techniques. They achieve this by modeling a small group of atoms (as in the AA systems) as a single particle (for CG systems) and maps the complex system with reduced degrees of freedom [134-138]. Modeling has moved from AA simulations to CG due to the fact that they are prohibitively expensive to study large deformation at larger length scales and have longer simulation time requirements compared to CG modeling. By decreasing the degrees of freedom, CG models increase the length and time scales of simulations and provide an efficient approach to simulate and investigate systems properties and behaviors at mesoscale.

CG models have been utilized and continuously improved in countless studies. Specifically, several recent studies from Dr. Meng's group have demonstrated that CG MD offers a great advantage than continuum-scale simulations and all-atomistic MD simulations [48, 139-145]. In bio-mimicry material advancement of mechanical properties, significant work has been conducted with promising results that show improved material properties and improved affinity between experimental and computational experiments that previously had discrepancies [146-151].

3.2 CG Model of NFC

The interfibrillar mechanics in CG models depend on the overlap length and their interactions. To properly capture these complex interactions, the shear lag model has been developed to depict the inter-fibril mechanics which is the foundation of the research [112, 152-154]. Mesoscopic features such as cellulose alignment, length, and orientation which has been shown to have extreme importance to mechanical properties, cannot be easily captures with single-scale atomistic approaches as shown in Figure 6 below. The prevalence of interfaces and the nanoscopic scale of CNCs/NFCs has further hindered continuum mechanical modeling of these systems.

Address these pitfalls in computational model, Qin et al. established a CG bead-spring model with a brick-and-mortar representation [144] that allows for the extension of simulation length and time scales. They conducted uniaxial tensile loading tests with varying lengths and interfacial energies to assess the mechanical performance that later resulted in models verified by experimental results. Because this model only utilized equilibrium conditions and strain energy conversation principles as determinate parameters for the CG model the atomistic interactions and mechanical property predictions were preserved. By using the strain energy conservation approach, they were able to capture the anisotropic mechanical properties of aligned CNC films consistently including Young's modulus, strength, and failure properties. The model successfully bridged the gap between atomistic and continuum models of mesoscopic scales at significantly higher computational efficiency. This novel model was developed further in our research to include defects and how that effects mechanical strength as explained

later in Chapter 4-5. Similarly, we were able to capture how bio-inspired idealized brick-and-mortar structures are dependent on overlap length and interfacial energy commonly found in cellulose.

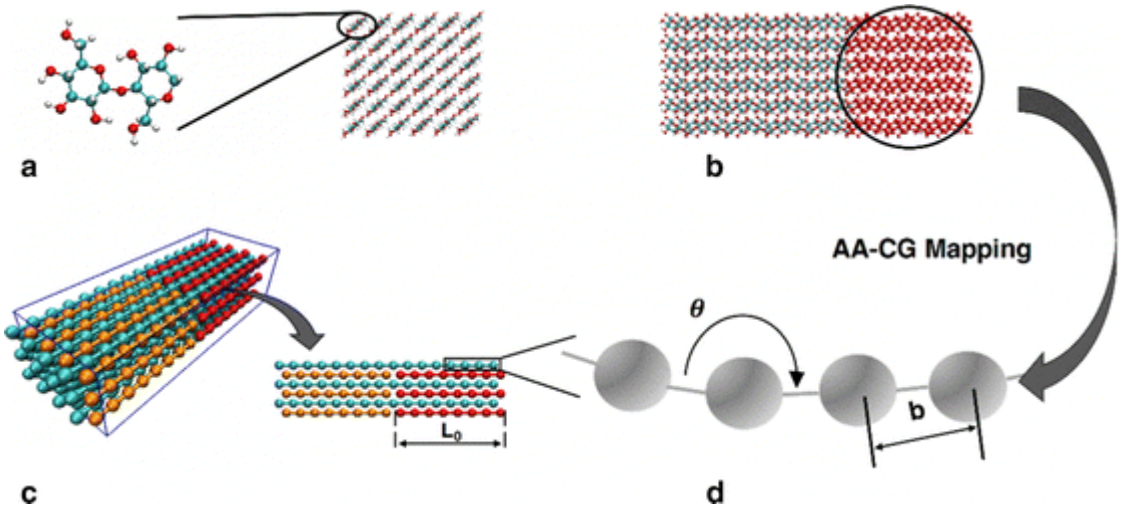

FIGURE 6: Hierarchical modeling of CNC nanopaper. (a) all-atomistic representation of CNC repeat units and the 36-chain cross-sectional structure of a CNC with (110) surface; (b) a representative CNC with highlighted and circled atoms making up 3 repeat-units on each chain, corresponding to a single CG bead in our model; (c) CG bead-spring mesoscale model for CNC; (d) CNC nanopaper structure showing the nacre-inspired layered structure (3D view), with highlighted single layer showing brick-and-mortar arrangements of CNCs with overlap length L_0 (top view). Reprinted from Qin *et al.*, *Cellulose* 2017 [144].

3.3 Shear Lag Model for Inter-Fibril Mechanics

A shear lag model is formulated to predict the stresses in a unidirectional fiber reinforced composite. The model is based on assumptions consistent with the finite element method and the principle of virtual work by assuming that the matrix displacements can be interpolated from the fiber displacements. The fibers are treated as one-dimensional springs and the matrix is modeled as three-dimensional finite elements. The resulting finite element equations for the system are transformed into differential

equations by taking the discretization length to approach zero. The governing ordinary differential equations are solved using Fourier transformations and an influence function technique [155]. A statistical shear lag model is derived by extending the classical shear lag model to account for the statistics of the constituents' strength. A general solution emerges from rigorous mathematical derivations, unifying the various empirical formulations for the fundamental link length used in previous statistical models [156].

To extend the statistical shear lag model for evaluating the strengths of higher order composites, the mechanical behavior of the unit cell was inputted to investigate how the size a of macroscopic composite is related to its strength. The first step to adapt the model, we must make the unit cell (when length $L \geq \tilde{L}$) was simplified to an element consisting of two sub-elements connected in series; where each element represents filament rupture and the other represents filament-filament sliding (shown in Figure (7) below). Consequently, a hierarchical composite comprised of $M \times .N$ unit cells can be simplified into the statistical model comprised of $M \times .N$ elements. The cross-section of the composite is modeled as a Daniels' bundles of M parallel unit cells aligned in the lateral direction that are clamped at both ends [157].

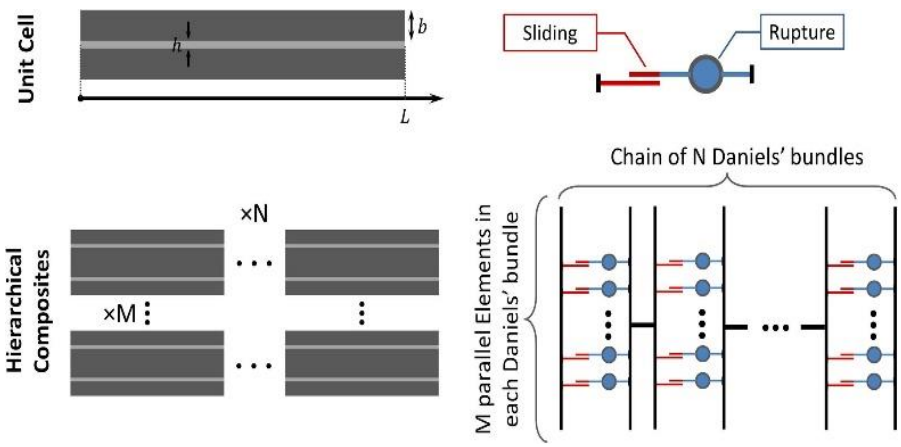

FIGURE 7: Schematic of method to scale up Statistical Shear Lag Model. Adapted from Wei et al, *Acta Biomaterials* 2015 [156].

Since we are along the axial direction, the composite is simplified into a chain of N Daniels' bundles connected in so that the composite has a total length defined by $L_{comp} = N \cdot L$. Furthermore, Daniels' theory suggests that the strength of a bundle comprised of M unit cells whose strength distribution is a Weibull probability function that exhibits a Gaussian distribution. Clearly, there is a size effect with respect to the strength of composites with different hierarchies as a function of the filament material, the unit cell, and the composite size.

The elastic solutions presented are the same as the well-known "shear-lag model". Which shows a typical distribution of the shear stress and tensile stress along the overlapped length. The shear stress maximizes at both ends and decreases exponentially toward the center, but the efficiency of the shear transfer drops, as a major portion of the overlapped region does not carry much shear load. Since the shear transfer mechanism is the key to understanding the mechanical properties of composites, it is important to quantitatively evaluate shear transfer efficiency. Here the elastic strain energy density is used to assess the shear transfer efficiency. Therefore, to maximize the elastic strain

energy density, one has to maximize $f(\lambda L)$. Solving numerically suggests that $f(\lambda L)$ has a maximum at $\lambda L \approx 3.28$, i.e., when the overlap length equals [112]

$$L^* \approx 2.318\sqrt{\frac{Ebh}{G}} \tag{1}$$

and

$$L^{**} = \frac{\sigma_f}{\tau_f} b \tag{2}$$

This characteristic overlap length, L^*, has the physical meaning at which the unit cell maximizes its elastic strain energy density (i.e., the shear transfer efficiency). The elastic solution discussed in the previous section provides a critical length that optimizes the total elastic strain energy density of a composite. It is worth noting that in the elastic region the length scale where the total elastic strain energy density is maximized differs from that at which the composite is optimized in strength. For a composite with a brittle interface (linear elastic shear behavior until failure), the elastic strain energy density of the material is still maximized at the characteristic length, L^* [157].

Therefore, to optimize the composite performance in terms of both toughness and strength, the ductility of the interface material also plays an important role, as discussed in the context of the plastic solution. By tailoring the plastic properties of the interface material, the effective strength of the composite materials can be optimized in the second characteristic overlap length, L^{**}, which is usually larger than L^*. Naturally, as the properties of the interface material are tailored such that L^{**} approaches L^*, the toughness and strength of the composite are simultaneously optimized. In the following, this hypothesis is verified by comparing the model's predictions for the overlap lengths

of three typical natural materials and those experimentally observed to occur in nature. Those natural materials include nacre shells [158], collagen in tendon/bone [159], and spider silk [160].

These characteristic length predictions have been verified successfully through experiments in three well-known composites, with varying geometries that range from micrometer down to nanometer scale. The model serves as a guideline in designing novel composite materials. Furthermore, *in situ* shear experiments on pristine Multi-Walled Carbon Nanotubes (MWCNTs) confirm the numerical model capability to describe load transfer between constituents. In the future, the shear experiment and numerical model introduced in this study can serve as valuable tools for designing high-performance carbon-based nanocomposites [112, 161]. Due to the success of these models and their simplification for our specific research purposes, this characteristic length was used in modeling the Bouligand nanocellulose microstructures.

3.4 Impact Resistance of nanocellulose films with Bouligand structures

One previous computational study, by building upon the CG model of NFC and understanding of the inter-fibril mechanics, provided insights into the dynamic failure mechanisms of a Bouligand-structured film made of continuous NFC. They found the impact resistance of such films strongly depended on γ, and a low γ (18°-42°) resulted in improved impact performance due to greater nanofibril sliding, crack twisting, and impact stress, significantly outperforming other pitch angle and quasi-isotropic baseline structures [48]. They found new insights into the importance of uniform wave propagation with minimal CNC rupture have been shown to help maintain film integrity

during impact. Furthermore, decreasing the interfacial adhesion energy of CNCs effectively enhances their impact resistance and energy absorption, and this effect is more pronounced for Bouligand microstructures with optimal pitch angles. They can enhance impact performance by readily admitting dissipative inter-fibril and inter-layer sliding events without severe fibril fragmentation.

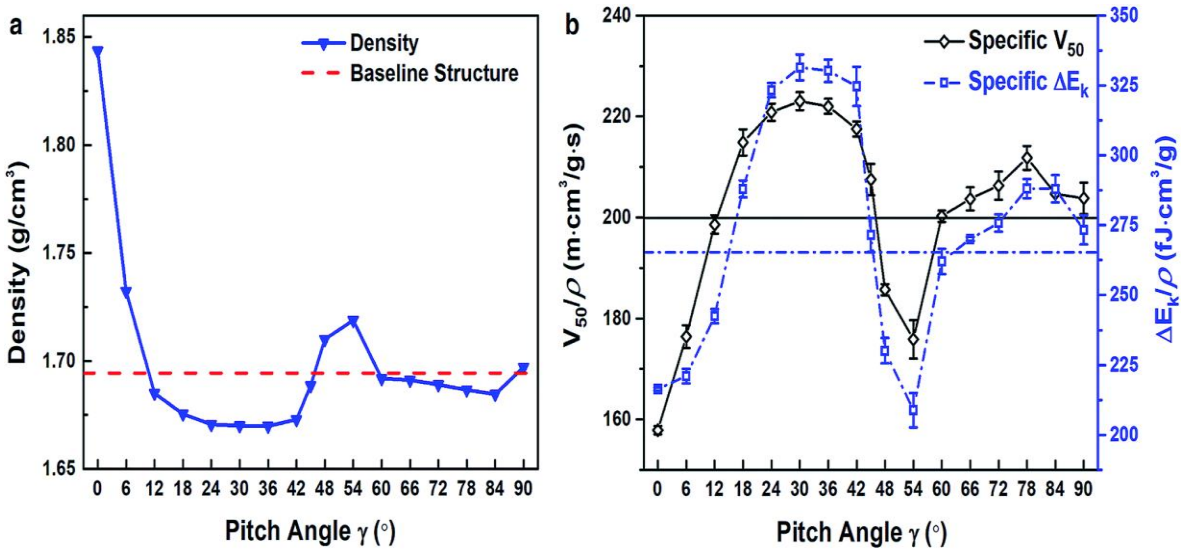

FIGURE 8: Continuous Bouligand microstructure density, ballistic limit, and energy absorption simulation results. (a) Density profile versus pitch angle and (b) specific ballistic limit velocity (V_{50}/ρ) in black and specific penetration energy ($\Delta E_k/\rho$) in blue respectively. Reprinted from Qin et al, *Nanoscale Advances* 2019 [48].

This work helped to reveal structural and chemical factors that govern the optimal mechanical design of Bouligand microstructures made from high aspect ratio nanocrystals, paving the way for sustainable, impact resistant, and multi-functional films; however, there are still limitations and gaps in our understanding of the Bouligand microstructures.

3.3 Remaining Knowledge Gap

In the study discussed in the last section, the authors showed that greater fibril sliding could contribute to the higher impact resistance of Bouligand-structured film made of continuous NFC summarized in Figure 8. However, the possible sliding events are intrinsically limited by the continuous nature of nanofibrils that span the whole film. It is reasonable to hypothesize that using short/discontinuous nanofibrils can potentially promote the fibril sliding. The selection of short/discontinuous NFC is motivated by the fact that NFC from wood, bacterial and plant cellulose biosynthesis process generally have lengths in the range of 500-2000 nm [162, 163]. By further conserving the critical crack twisting mechanisms by judicious selection of discontinuous sites and γ, the overall impact resistance of the CNC films can possibly be enhanced.

A recent study partially validates this hypothesis by applying a hybrid Bouligand and nacreous staggered structures, named discontinuous fibrous Bouligand (DFB) architecture, and examining the fracture energy of 3D-printed single-edge notched specimens. The study showed that this DFB architecture achieves enhanced fracture resistance due to the hybrid toughening mechanisms of crack twisting and crack bridging mode [49]. Remarkably, other previous studies demonstrated that cracking twisting and crack bridging may coexist during the fracture process of natural materials with Bouligand structures [164-169]. A few other studies have also shown that hybrid designs that combine different microstructures can break performance tradeoffs and improve fracture toughness [76, 115, 116].

However, whether such hybrid designs by combining Bouligand and staggered structures could lead to enhanced impact resistance under localized projectile impact remains unknown, and how to design nanocellulose films with NFCs as building blocks to achieve the optimal impact resistance is a daunting challenge as a larger number of design parameters can affect the final performance.

I aim to answer the question and address this challenge in this thesis by building upon previous studies on model development and simulations. In the next chapter, I will first introduce the computational models and methods used in this thesis.

CHAPTER FOUR

COMPUTATIONAL MODELS AND METHODS

In this chapter, I will discuss the computational model and methods to systematically investigate the dynamic failure mechanisms and quantify the impact resistance of NFC films that adopt a DFB architecture, i.e., staggered discontinuous NFC in each layer with a helicoidal layup, by leveraging CGMD simulations. By carrying out explicit projectile impact MD simulations and characterizing the ballistic limit velocity (V_{50}) and penetration energy (ΔE_k), we examine the impact resistance of NFC films with DFB architecture depending on different geometric factors. We also characterize the deformation mechanisms that affect the impact resistance from simulation trajectories.

4.1 Overall Model Setup

Our model system is illustrated in Figure 9, where we highlight the simulation scheme, DFB architecture, and the CG model used for the NFC building block. As previously discussed, Bouligand-architecture films with continuous fibrils have been previously studied, and their mechanical properties under different loading conditions have been summarized [48, 144]. The difference between continuous NFC and discontinuous NFC is manifested at the red beads, where fibrils are disconnected by deleting the intra-fibril interactions (bond and angle interactions). The length *L* represents the whole length of the fibrils, and all the fibrils have constant *L* in each simulation case. We alter *L* for different cases and systematically study its effect on the impact resistance of the NFC films with DFB architecture. All the projectile impact simulations are carried

out using the Large-scale Atomic/Molecular Massively Parallel Simulator (LAMMPS) [170]. The simulation trajectories are visualized by the Visual Molecular Dynamics (VMD) program [171].

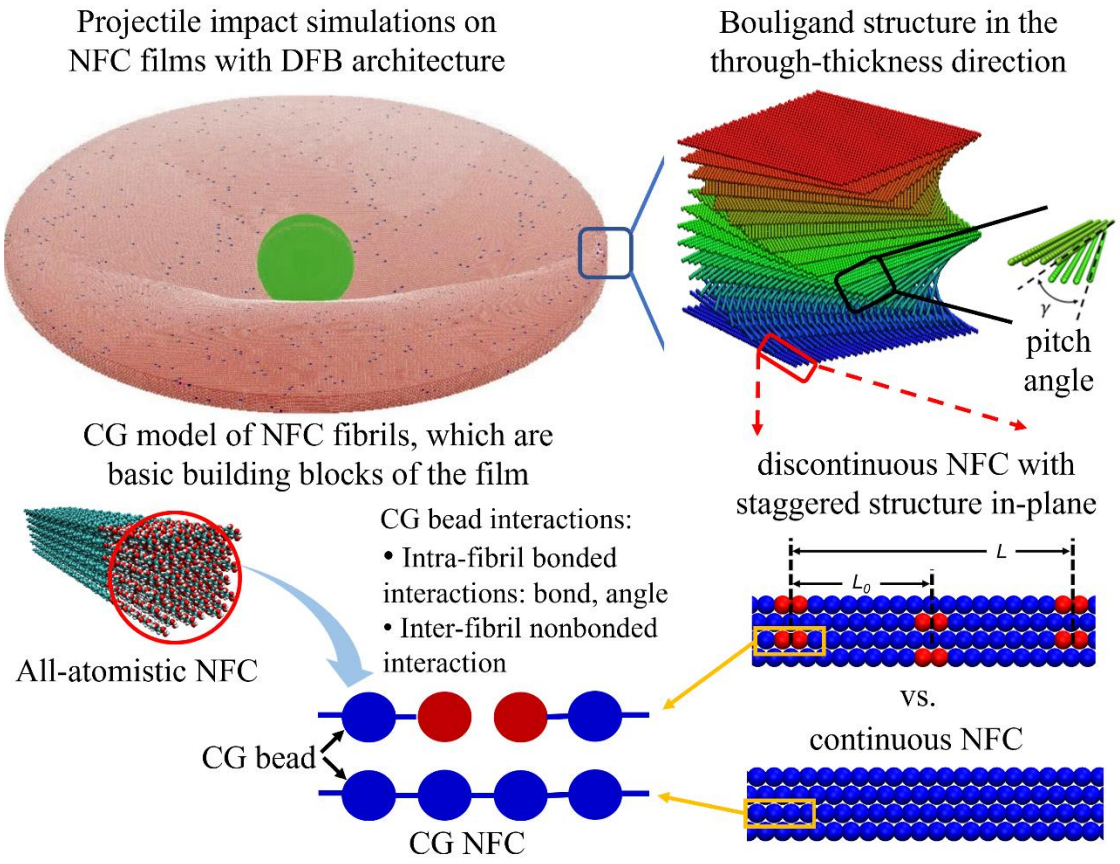

FIGURE 9: Simulation schematic and structural design for NFC films with DFB architecture.

LAMMPS provides more versatility in performing specific simulation techniques than other software which is why it is utilized in this study. Time steps in LAMMPS are used $1/10^{th}$ the time of the fast period of relevant motion of the system, and with CG models it allows for an increase in time step.

4.2 Bead-Spring Mesoscopic CG Model

The all-atom CNC structure has been mapped onto the multi-bead chains. The bead-spring mesoscopic CG model is the foundation of the simulations utilized in this research and have been verified through previous experimental results. In Figure 9 above, the DFB architecture is structured through-thickness in this Bouligand orientation and through the simulations it was determined the best pitch angle between each ply of the film. Further analyzing the bead formation utilizing the shear-lag between beads of each fibril. In these simulations, the "defects" are modeled through non-interacting intra-fibril bonded beads. Previous studies conducted, utilized continuous intra-fibril bonded beads which is the primary difference between that study and the study conducted here [48].

The model system builds upon the previously established bead-spring mesoscopic CG model of NFC [144]. Within this model, each CG bead represents three repeat units of the 36-chain structured (110) surface of NFC. The diameter of each CG bead is 3.4 nm, making its cross-sectional area equal to that of the NFC. Those CG beads interact with each other through bonded and non-bonded interactions. The bonded interactions include harmonic bonds and harmonic angles whose potential functions are shown below:

$$V_{bond} = k_b(b - b_0)^2 \text{ for } b < b_{cut} \quad (3)$$

$$V_{angle} = k_\theta(\theta - \theta_0)^2 \quad (4)$$

where k_b is twice the spring constant, b is the bond length, b_0 is the equilibrium bond length, k_θ is twice the bending spring constant, θ is the bending angle, and θ_0 is the equilibrium bending angle which is set to $180°$. For the bond potential, a cutoff b_{cut}=3.27 nm is set as the failure criterion corresponding to a failure strain of 5% based

on prior MD studies [172]. The other values of bond potential parameters and angle potential parameters are determined through uniaxial tension and three-point bending tests on the AA model of NFC, respectively, according to the strain energy conservation approach. The values of those parameters can be found in Table 1. The non-bonded interaction is incorporated to account for the electrostatic and van der Waals effects. In this CG model, a Morse potential is employed to model the non-bonded interaction:

$$V_{nonbonded} = D_0[e^{-2\alpha(r-r_0)} - 2e^{-\alpha(r-r_0)}] \quad (5)$$

where D_0 is the well depth, α controls the width of the potential well, r is the distance between two beads, and r_0 is the equilibrium distance. The values of the parameters in the Morse potential are determined by matching the interfacial properties between the CG and AA models and are presented in Table 1. Further, a cutoff distance $r_{cut} = 6$ nm is set to consider only neighboring inter-fibril interactions and increase computational efficiency.

Table 1. The Parameter Values Used for the Bond, Angle, and Non-Bonded Potentials.

Parameter	Value	Parameter	Value
b_0	31.14 Å	k_b	$260\ kcal \cdot mol^{-1} \cdot Å^{-2}$
θ_0	180°	k_θ	$77000\ kcal \cdot mol^{-1} \cdot rad^{-2}$
r_0	36 Å	D_0	$240\ kcal \cdot mol^{-1}$
α	$0.3\ Å^{-1}$		

Building upon the validated model of NFC, we construct representative NFC films using 11 layers (approximately 37 nm in thickness) of parallelly staggered NFC in

each layer with left-handed helicoidal structures that are typical of chitin-rich shells of crustaceans and self-assembled NFCs [31, 32, 51, 164]. Specifically, a rotational angle, γ, about the axis normal to the layer plane is assigned starting from the bottom-most layer. In this study, the following γ are considered: 0°, 18°, 30°, 45°, 75°, and 90°. We note that the number of layers and selected γ are consistent with our previous study on continuous NFC film [48]. Discontinuous NFCs are constructed from continuous fibrils spanning the whole length of each layer by deleting the bonded interactions between the beads at the discontinuous sites (Fig. 9). We note that actual discontinuous sites can be larger than that considered herein. However, we believe the impact resistance of NFC films is mainly governed by the overlap length of nanofibrils when the size of defects is much smaller compared to the length of nanofibrils and the size of the projectile. Therefore, we believe the results in this study are generalizable to films with potentially larger defect sizes. There may have multiple discontinuous sites over the span of the impact region depending on the lengths and specific configurations selected in this study, which are discussed later.

4.3 Discontinuity Configuration Setup

We have selected four configurations regarding the location and distribution of discontinuous sites while keeping a unified length ($L = 500\ nm$) for all nanofibrils. For the first three patterns (Figure 10 (a)-(c)), adjacent nanofibrils in each layer have a 50% overlap length, and thus, the distance between discontinuous sites (L_0), e.g., the overlap length, is half of the fibril length L.

The first configuration is denoted as Offset since we shift the discontinuous lines away from the impact site by 50% of the L_0 for each layer. The top view (Figure 10 (a)) shows the discontinuous lines are offsite from the center of the film. We note that we further alter L using the Offset configuration and study the influence of L in the later part of this paper. The second configuration is denoted as Middle (Figure 10 (b)) as one line of discontinuous sites in each layer crosses the center of the impact zone. From the top view of the $\gamma = 0°$ case, we can clearly see the discontinuous sites lying in the middle. For the third configuration, named Random Through-Thickness (TT) (Figure 10 (c)), we shift the discontinuous sites for each layer collectively in-plane with a random distance between 0 and 50% of the L_0 based upon the Middle configuration. We note that the adjacent nanofibrils in each layer still have a 50% overlap length. This 50% overlap pattern can be seen from the top view of a specific layer in Figure 10(c). In the last configuration, Random In-Plane (IP) (Figure 10(d)), we further introduce randomness for overlapping lengths between adjacent fibrils in-plane. In this case, the smallest overlap length governs the mechanical strength along the fibril direction for each layer [91].

Even though the four selected configurations cannot represent all possible configurations for NFC films, we believe such selections can help us to understand the effects of the location and distribution of discontinuous sites on the ballistic impact resistance of NFC films in this study.

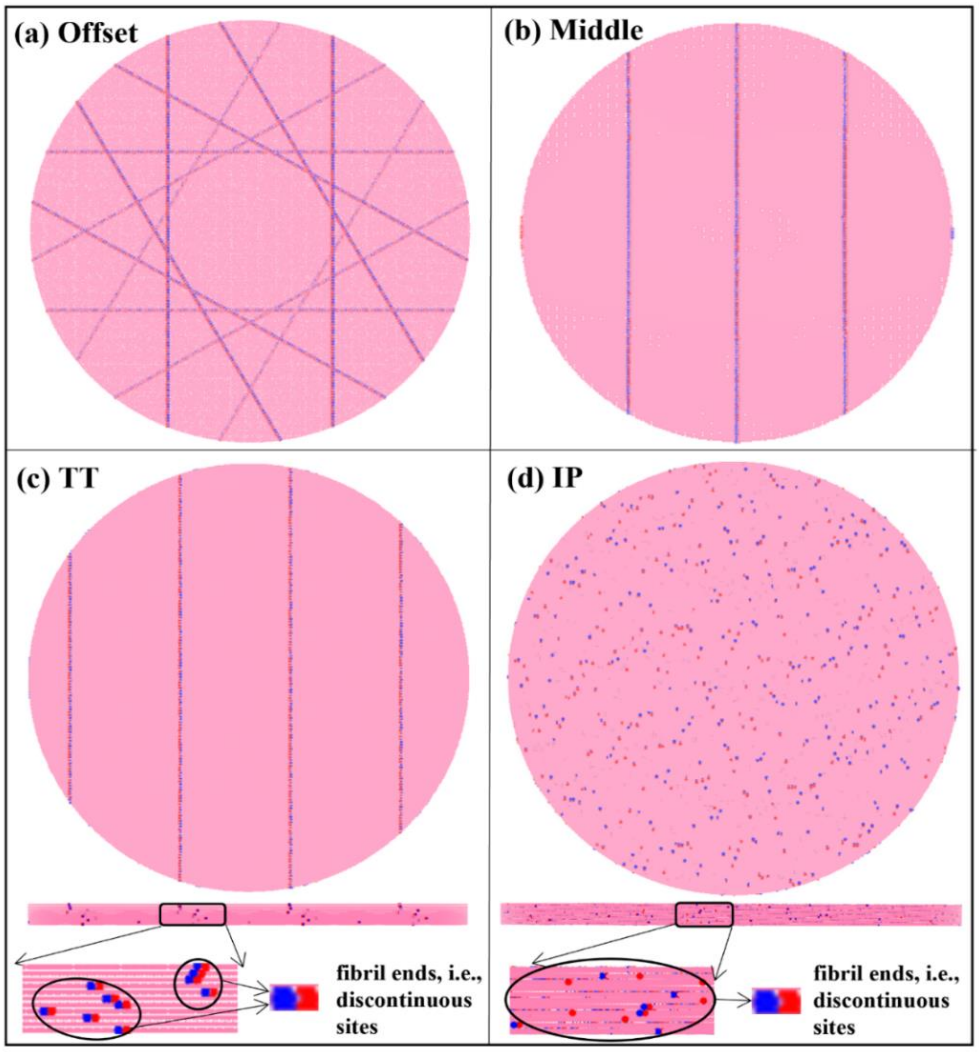

FIGURE 10: Different configurations considered in this study. (a) Top view of the Offset configuration film ($\gamma = 30°, L = 750$ nm), **(b)** top view of Middle configuration film ($\gamma = 0°, L = 500$ nm), **(c)** top view of the top layer and side view of the film for the Random TT configuration ($\gamma = 0°, L = 500$ nm), **(d)** top view of the top layer and side view of the film for the Random IP configuration ($\gamma = 0°, L = 500$nm). The blue and red dots represent fibril ends or discontinuous sites.

4.4 Detailed Simulation Procedures

We define an impact region of the NFC film that has a diameter of 1,000 nm. We note that a fibril length of 2,000 nm in the Offset configuration is identical to a continuous nanofibril case as the discontinuous sites will be all outside of the impact

region. An explicit projectile is also fixed 10 nm above the geometric center of the impact region of the NFC film to avoid possible interactions. The projectile is in a spherical shape with a diameter of 160 nm and consists of CG beads that are arranged in a cubic diamond pattern. The density of the projectile is 3.53 g/cm^3. The interactions between the projectile beads and the NFC beads are modeled by a 12-6 Lennard Jones (LJ) potential [145]:

$$V_{LJ}(r) = 4\varepsilon_{LJ}\left[\left(\frac{\sigma_{LJ}}{r}\right)^{12} - \left(\frac{\sigma_{LJ}}{r}\right)^{6}\right] \quad (6)$$

where r is the distance between a projectile bead and a Bouligand bead. The two parameters, ε_{LJ} and σ_{LJ}, are chosen to be 20 kcal/mol and 4 nm, respectively. Our previous study shows that the value of ε_{LJ} has a negligible influence on the ballistic impact response of the Bouligand structure, but a high value may bring more noise to the force responses at high impact velocities [143]. Such settings are consistent with our previous study on continuous NFC films [1].

During the impact process, the NFC beads outside of the impact region are fixed, resembling the clamping boundary condition in previous experiments [173]. The NVE (microcanonical) ensemble is adopted during the impact process. The projectile is set rigid as there is no obvious deformation of the projectile during such micro-ballistic impact tests [89]. An initial velocity perpendicular to the film is given to the projectile to initiate the impact process. In determining the V_{50} of the different NFC films, a series of initial velocities are assigned to the projectile in the trial tests, and we look for the lowest velocity to fully penetrate the film, which is our selection of V_{50}. To calculate ΔE_k, we

use impact velocities that are higher than V_{50} of the films. Specifically, we have used three velocities, 400 m/s 500 m/s, and 1000 m/s, to measure ΔE_k. For the purposes of measuring V_{50} and ΔE_k with higher reliability, multiple simulations have been run for each case, and we take the average value to report/plot and include the standard deviations as error bars.

CHAPTER FIVE

RESULTS AND DISCUSSION

In this section, we first study the effect of different configurations and identify a more representative configuration (Offset) for detailed examinations of the deformation mechanisms. We then highlight a few cases that show enhancement in impact resistance over the continuous fibril case. Next, we analyze the effects of pitch angle (γ), fibril lengths (L), and other factors on the dynamic deformation mechanisms of NFC films under projectile impact and discuss their roles in altering the failure mechanisms and impact resistance. Our previous study has shown that NFC films with different γ show non-negligible differences in film density (ρ) [48]. Therefore, we use the specific ballistic limit velocity (V_{50}/ρ) and penetration energy ($\Delta E_k/\rho$) to assess the impact resistance of different NFC films.

5.1 Effect of Different Configurations on Impact Resistance and the Role of Impact Velocities.

Projectile impact simulations were first conducted on all four configurations as they provide a wider scope of impact failure mechanisms to study within the NFC films. By comparing their performance in terms of V_{50}/ρ and $\Delta E_k/\rho$, we aim to determine a suitable initial impact velocity for assessing $\Delta E_k/\rho$ of different films and look into the influence of specific configurations on the films' impact resistance.

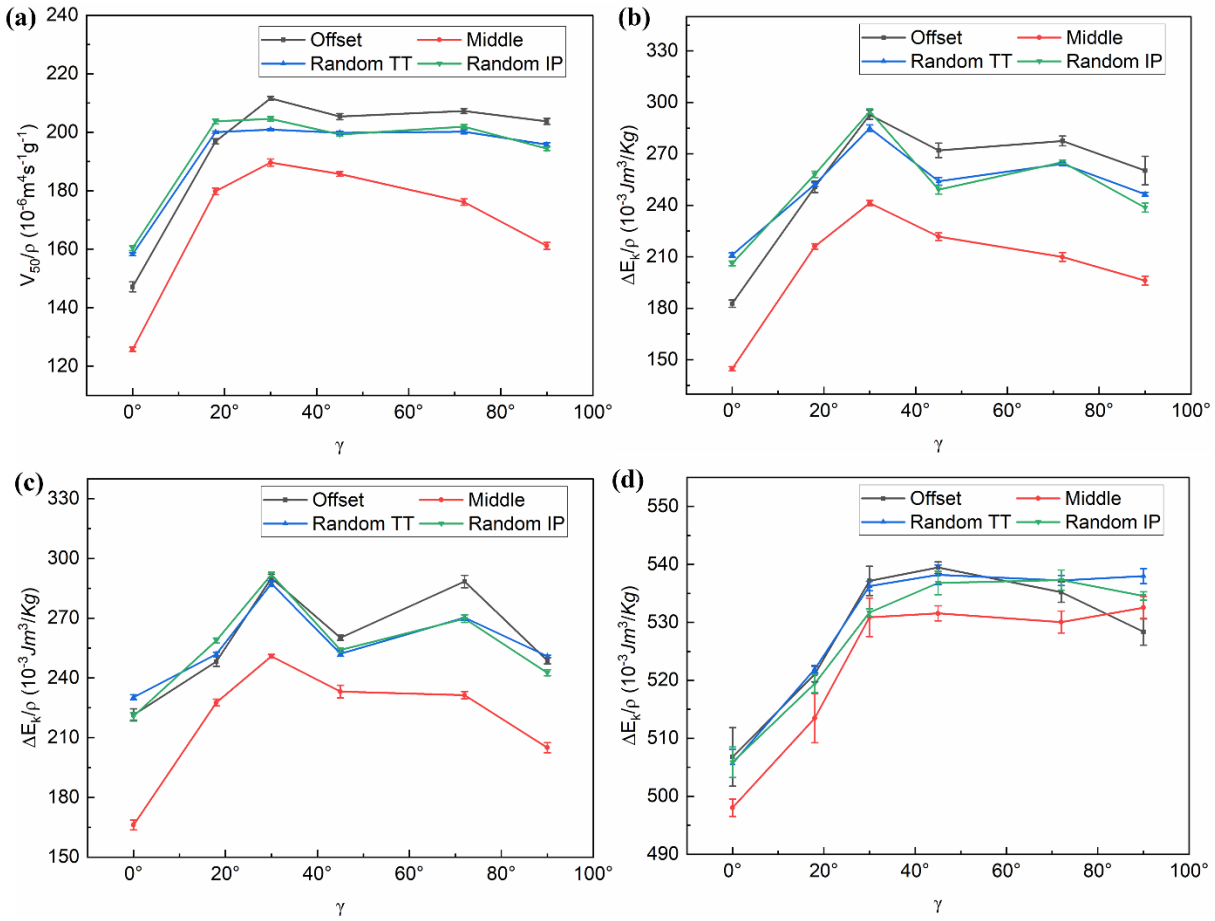

FIGURE 11: Summary results for different defect orientations. V_{50}/ρ **(a)** and $\Delta E_k/\rho$ of NFC films with different DFB configurations and constant $L = 500\,nm$ at initial impact velocity of 400 m/s **(b)**, 500 m/s **(c)**, and 1000 m/s **(d)**. The error bars mark the standard deviations from five simulation runs.

Figure 11 compares the impact resistance of NFC films with different configurations and constant $L = 500\,nm$. Figure 11 (a) plot of V_{50}/ρ results and Figure 11 (b)-(d) show $\Delta E_k/\rho$ results at three different initial impact velocities for all different configuration cases considered herein. We find that V_{50}/ρ results (Figure 11(a)) exhibit similar trend to $\Delta E_k/\rho$ at impact velocity of 400 m/s (Figure 11(b)). We also find that the energy absorption level of the films cannot be discriminated against under an impact

velocity of 1000 m/s (Figure 11(d)). Under high-velocity projectile impacts, films primarily absorb energy through local tearing around the projectile rim and fragmentation within the projected volume, while energy absorbed through other failure mechanisms is negligible. This phenomenon happens when the films are not able to delocalize the high stress at the impact site to a larger deformation zone before local penetration [142]. By considering V_{50}/ρ as an intrinsic impact resistance characteristic, our results show that $\Delta E_k/\rho$ at lower initial impact velocity reflects the intrinsic impact resistance of NFC films. This observation is consistent with our previous study on 2D materials and polymer thin films [142]. Therefore, we select the initial impact velocity of 400 m/s to compare $\Delta E_k/\rho$ of NFC films with different structures in the rest of this study.

Then, we investigate how different configurations affect discontinuous films' impact resistance. Figure 11 (a) and (b) show that the Offset configuration films have the highest V_{50}/ρ and $\Delta E_k/\rho$ than other films at a large range of pitch angles considered herein, and films with the Middle configuration having the worst performance in terms of V_{50}/ρ and $\Delta E_k/\rho$. These results indicate that the Offset configuration can lead to enhanced impact resistance in general. Intriguingly, films with Random TT and Random IP configurations are superior at lower pitch angles like 0° and 18°. By examining the simulation trajectories, we find that Random TT and Random IP films uniquely utilize fibril breaking near the edge of the film to absorb energy, as shown in Figure 12 (a) and (b). Additionally, the Random TT film shows crack bridging mechanisms in the through-thickness direction as the discontinuous sites are randomly shifted among different layers. Furthermore, it is expected that more fibril sliding events can occur in the Random IP

film at small pitch angles as the smaller overlap length can lead to smaller energy barriers of fibril sliding. We should also note that the superior performance of Random IP and TT configurations compared to the Offset at lower pitch angles may also be due to the specific L used herein, when the fibril sliding and crack bridging mechanisms aforementioned contribute significantly to the intrinsic impact resistance. With a different L, their contribution likely changes, and the effect of configurations on impact resistance can be altered as well.

Because the Offset configuration outperforms other configurations in a broader range of γ and has a more deterministic fibril overlap length and structural pattern, we focus on the Offset configuration in the next section. Specifically, we conduct a thorough investigation into the effects of L and γ and expand the discussions on the roles of different failure mechanisms in the subsequent sections.

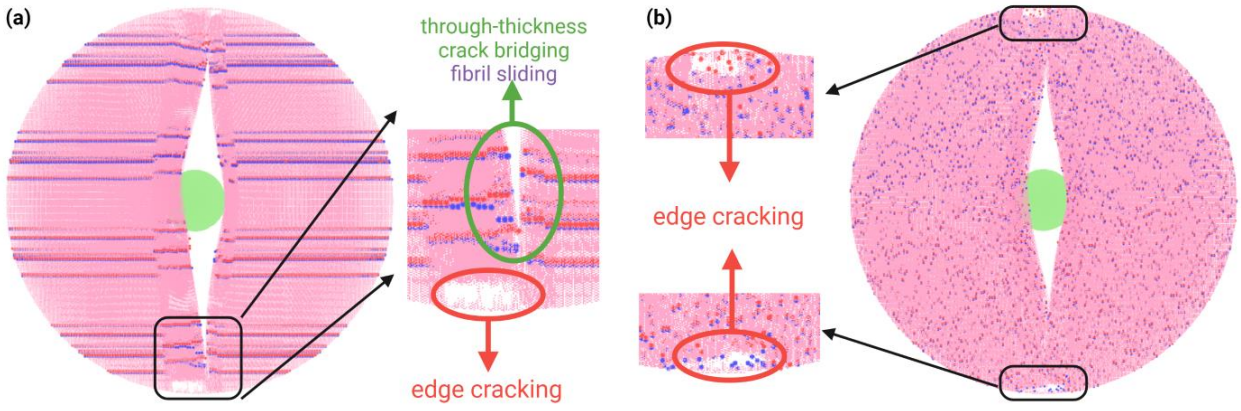

FIGURE 12: Top view of failure mechanisms. Top view of films with **(a)** Random TT and **(b)** Random IP configurations with γ =0° and L =500 nm. The insets highlight the failure mechanisms – edge cracking, through-thickness crack bridging, and fibril sliding – present in these two configurations.

5.2 Impact Resistance of NFC Films with Offset Configuration.

We characterize and compare the impact resistance of NFC films with Offset configuration and varying L in the range of 50-1750 nm. Specifically, we measure V_{50}/ρ and $\Delta E_k/\rho$ at 400 m/s of different films and investigate the detailed failure mechanisms during the impact process. To compare the impact resistance of NFC films with DFB architecture and those with continuous nanofibrils, i.e., consisting of Bouligand architecture only (from our previous study [48]), we can examine whether the DFB architecture with hybrid Bouligand and staggered structures has an advantage over Bouligand architecture only.

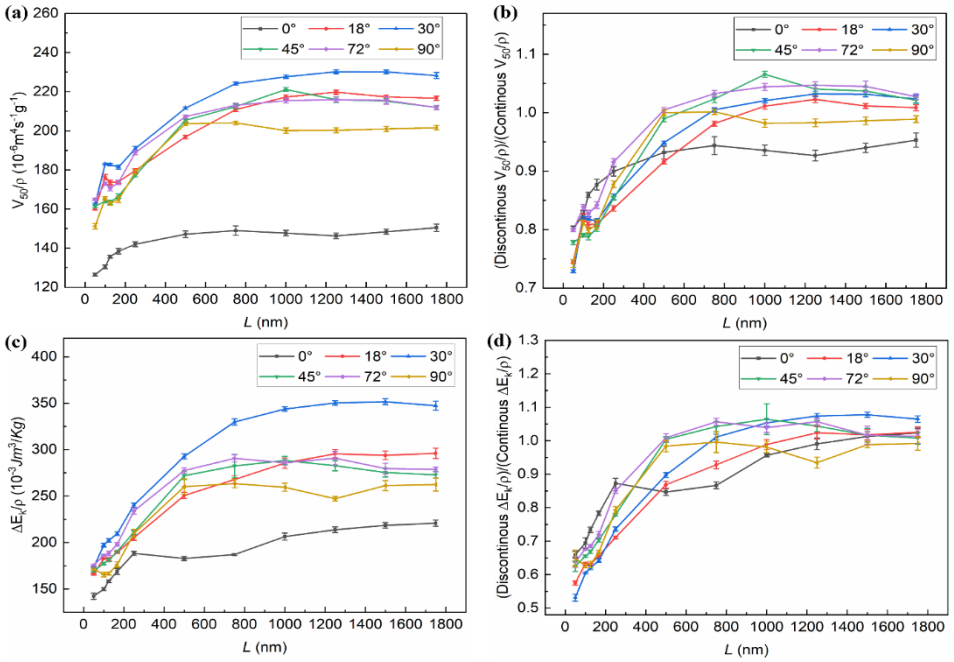

FIGURE 13: Summary results for different pitch orientations and fiber lengths. The absolute **(a)** and normalized **(b)** V_{50}/ρ values of the NFC films with DFB architecture. The absolute **(c)** and normalized **(d)** $\Delta E_k/\rho$ values of the NFC films with DFB architecture at an initial impact velocity of 400 m/s. The error bars mark the standard deviations from five simulation runs.

The explicit values and trends of V_{50}/ρ and $\Delta E_k/\rho$ for NFC films with DFB architecture with different L (x-axis) and γ (different colors in the legend) are shown in Figure 13 (a) and (c). In Figure 13 (b) and (d), we further plot the normalized V_{50}/ρ and $\Delta E_k/\rho$ values, where the values in Figure 13 (a) and (c) are scaled by the corresponding values of continuous NFC films that have been obtained in our previous study [48]. Thus, a normalized value larger than 1.0 indicates better performance in impact resistance. It is worth noting that for the shortest $L = 50$ nm (i.e., $L_0 = 25\,nm$) used in this study, the overall impact resistance of NFC films with DFB architecture still achieves 50%~80% of that of continuous NFC films. Our previous study showed that with $L_0 = 25\,nm$, unidirectional NFC nanopaper can achieve approximately 50% of the stiffness and strength of the continuous counterparts [49]. We note that additional factors, such as Bouligand structures in the thickness direction and offset configurations, can also contribute to the overall impact resistance of NFC films made of relatively short nanofibrils. This observation further demonstrates the effectiveness of DFB architecture in achieving excellent impact resistance despite using relatively short nanofibrils.

Interestingly, most NFC films with DFB architecture and pitch angles ranging from 18° to 72° and L larger than 750 nm show improved impact resistance than continuous NFC films. Despite less than 10% enhancement, the results here are remarkable as we demonstrate discontinuous nanofibril assemblies can achieve greater impact resistance against localized, high-speed projectile impact than continuous fibril assemblies. This is counterintuitive as continuous (long) fibrils normally possess superior mechanical properties than discontinuous (short) fibril assemblies. Previous studies show

that discontinuous nanofibril/platelet assemblies can approach the mechanical strength and toughness of the continuous nanofibril/platelet assemblies as the length of nanofibril/platelet increases [144, 174]. Nevertheless, our study further demonstrates that by using discontinuous nanofibrils and adopting a DFB architecture, we can improve the impact resistance of NFC films compared to films made of continuous nanofibrils. Next, we look into the underlying mechanisms that explain the improved impact resistance.

5.2.1 Mechanisms That Lead to the Improved Impact Resistance of NFC Film with DFB Architecture.

When films undergo projectile impact, the presence of discontinuous sites allows the initiation of local cracks due to local high stress concentrations and fibril sliding starting at the discontinuous sites. Additionally, we have observed several toughening mechanisms, such as crack bridging and crack twisting, during the projectile penetration process in NFC films due to the hybrid design of Bouligand and staggered structures, as illustrated in Figure 13. We believe these toughening mechanisms contribute to the improved impact resistance of NFC films with DFB architecture compared to films with continuous fibrils. Previous studies showed that crack twisting and crack bridging were the two main toughening mechanisms, and the inclusion of discontinuous sites essentially increases the possibility for these failure mechanisms to occur [49, 166, 167]. It is important to note that these failure mechanisms are strongly correlated with each other, and some of them can happen simultaneously.

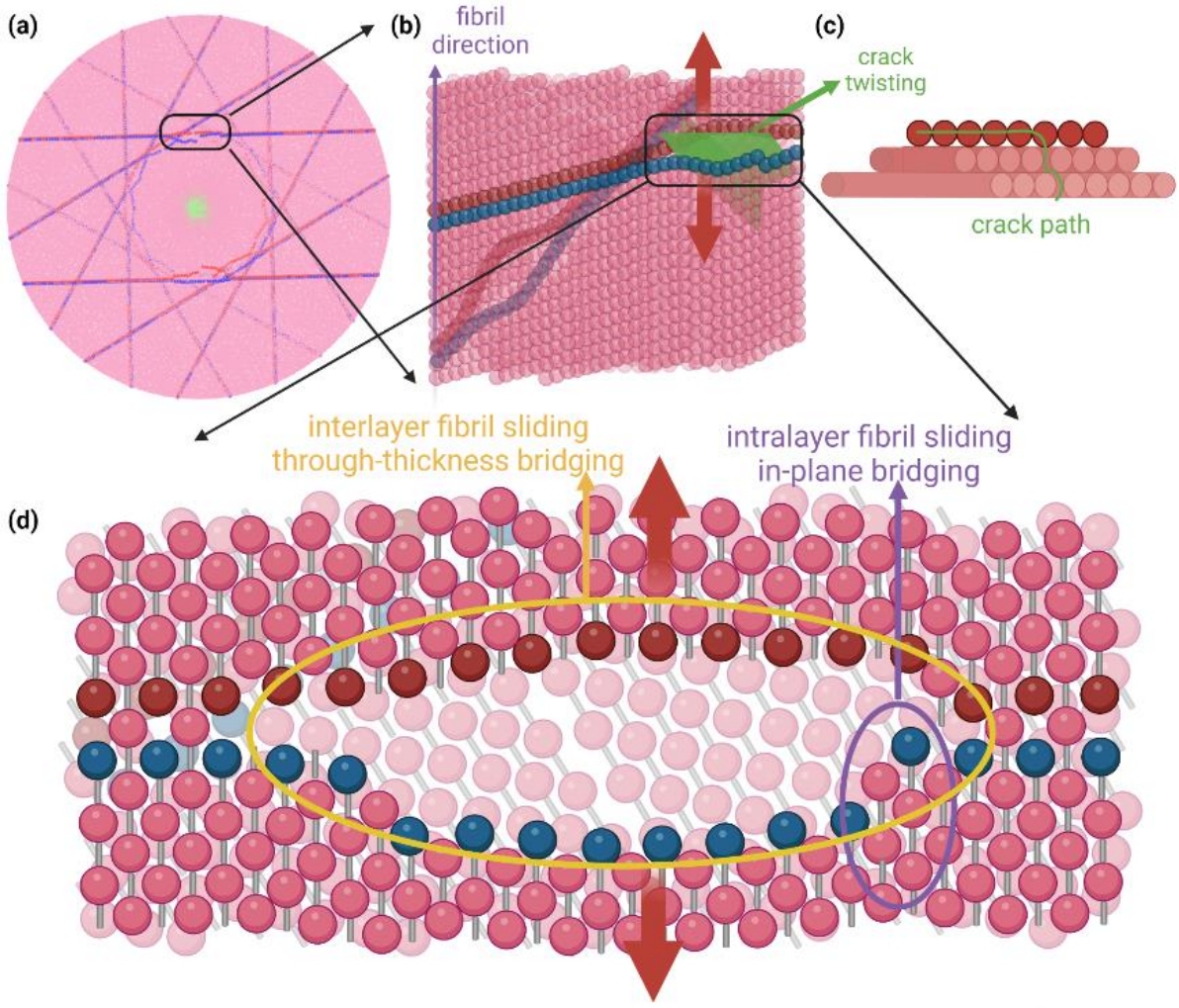

FIGURE 14: Diagram of interlayer fibril sliding during impact. (a) Bottom view (i.e., view from the back side) of the NFC film with Offset configuration, $\gamma = 30°$, and $L = 750$ nm. **(b)** A detailed sectional view of the film shows the deformation away from the impact site. **(c)** Demonstration of the long-twisted crack path due to crack twisting. **(d)** The enlarged schematic diagram highlights fibril sliding and crack bridging mechanisms.

More specifically, intralayer fibril sliding can initiate at discontinuous sites that are away from the impact site due to the development of the impact-propagation zone [142]. Such sliding events can help dissipate impact energy through inter-fibril frictions. Fibril sliding events may lead to intralayer crack opening within NFC films, which

usually involve the crack bridging mechanism resulting from the staggered nanofibrils (Figure 14 (d)). We note crack bridging mechanism promotes impact resistance of the films by dissipating additional impact energy when cracks propagate [140, 175]. In addition, crack bridging mechanisms also exist in interlayer deformation. As shown in Figure 14 (d), when the cracks propagate in the top layer as fibrils sliding, the fibrils in the layer below also function as bridges to decelerate the crack opening while dissipating energy. Moreover, interlayer fibril sliding and intralayer fibril sliding may compete with each other to occur, where the outcome is also influenced by the geometric factors of the films (i.e., L and γ), as discussed later. Previous studies have similarly shown that crack bridging mechanism alleviate stress from crack tips which allows stable growth of cracks instead of immediate propagation in an unstable (often catastrophic) fashion [54][56].

Crack twisting is another failure mechanism observed in a large portion of NFC films during projectile penetrations. Previous studies indicate that crack twisting is generated by small pitch angles between adjacent layers that direct cracks to propagate along longer paths and thus enhance the impact resistance of Bouligand architectures [108, 140, 176]. The twisted cracks follow the fibril orientations in Bouligand architectures. In the NFC films with DFB architecture, we find that the introduction of discontinuous sites that are interconnected but along different orientations because of pitch angles that have the potential to further increase the twisted crack paths. Figure 14 (b) demonstrates that as fibrils slide in the top layer, which results in the in-plane crack, the fibrils in the adjacent layer also start to slide following the orientation of discontinuous sites and lead to a crack opening in that layer. Then, the crack opens in the

next layer by following the same pattern so on and so forth, which creates a twisted crack with elongated crack paths, as illustrated in Figure 14(c). In summary, we find that in the NFC films with DFB architecture, fibril sliding across different layers triggers a combination of crack bridging and twisting mechanisms, which enable enhanced energy dissipation. Based on the findings here, we hypothesize that the enhancement in impact resistance by adopting DFB architecture can be potentially increased when the system size becomes even larger and additional hierarchies are introduced to the NFC films. We plan to test this hypothesis in our future study.

5.2.2 Effect of Fibril Lengths.

In this section, we discuss the effect of fibril lengths (L) on the energy dissipation of the NFC films with DFB architecture. According to Figure 13 (b) and (d), at most pitch angles, both V_{50}/ρ and $\Delta E_k/\rho$ at 400 m/s increase drastically as L increases from 50 nm to 750 nm and then saturate for longer fibril cases. The normalized V_{50}/ρ and $\Delta E_k/\rho$ follow a similar trend, and certain γ lead to better performance than the corresponding films with continuous fibrils, as discussed in previous sections. In this section, we mainly discuss the reasons that contribute to improved impact resistance as L increases initially.

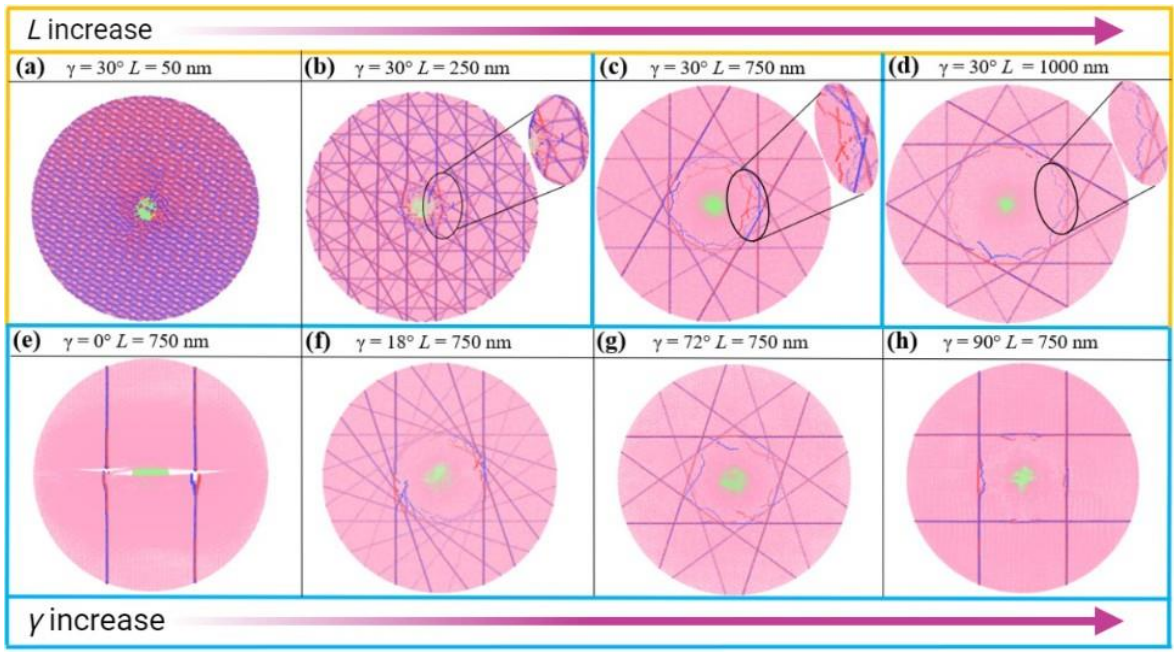

FIGURE 15: Bottom views of NFC films with Offset DFB configuration under an initial impact velocity of 400 m/s. In (b)-(d), the deformations away from the impact site are highlighted in the insets. The γ and L are specified for each film.

The stress distribution of a film under ballistic projectile impact was previously experimentally studied [177], and these experiments show that as a projectile makes initial contact with the film, the stress exerted on the impact site is the greatest. The magnitude of stress decreases radially towards the edge of the film. When L is small (i.e., below 200 nm), the impact site consists of high-density discontinuous sites, and thus it easily falls apart, and the impact resistance is significantly lower. Shown in Figure 15 (a)-(d), the number of discontinuous sites within the developed impact propagation zone during impact decreases as L increases from 50 nm to 750 nm and then completely disappears with a further increase of L. This likely explains the saturation of V_{50}/ρ and $\Delta E_k/\rho$ beyond $L = 750$ nm. We thus term $L = 750$ nm as the critical L in terms of impact resistance in our study case. From the simulation trajectory, we also find that

more significant fibril sliding away from the impact site can be observed as L becomes larger than 250 nm. Also, the fibrils tend to slide for longer distances in films with larger L. Moreover, films with larger L lead to longer twisted crack paths, which further enhances energy dissipation capability. In summary, NFC films with shorter fibrils (relative to the size of the projectile) mainly exhibit local deformation and penetration under the projectile impact, and the energy dissipation capability is limited. However, when the fibrils become significantly longer compared to the impact propagation zone, the NFC films can activate additional failure mechanisms such as fibril sliding, crack twisting, and crack bridging to enhance the energy dissipation capability.

5.2.3 Effect of Pitch Angles.

In this section, we discuss the effect of pitch angle (γ) on energy dissipation of the NFC films with DFB architecture. We focus on the films with L that exceed the critical L as the V_{50}/ρ and $\Delta E_k/\rho$ results saturate for larger L and show low standard deviations. We note that for these cases, the defects are away from the impact site and are scattered in terms of both intralayer and interlayer for non-0° γ cases. Figure 13 shows that γ plays a key role in the energy dissipation of the films, but unlike the effect of L, there is not a clear trend for impact resistance of the films with increasing γ. This finding is nontrivial as it cannot be simply explained by the concentration of defects and their proximity to the impact site. Specifically, films with γ ranging from 18° to 72° exhibit consistently higher V_{50}/ρ and $\Delta E_k/\rho$. Among these, the film with γ = 30° shows the greatest V_{50}/ρ and $\Delta E_k/\rho$, while the films with 0° pitch angle have the worst impact resistance. We note that our previous study with continuous fibrils showed similar results [52, 175]. Also, the

normalized V_{50}/ρ and $\Delta E_k/\rho$ at 400 m/s exceed 1.0 for films with γ ranging from 18° to 72° and L exceeding the critical L, as discussed previously. From our results, 30° is found to be the optimal γ for NFC films with DFB architecture. It is worth mentioning that when DFB architecture is subjected to different loadings, the optimal γ may vary [49, 178, 179].

We think it is also important to understand why NFC films with γ = 0° and 90° exhibit lower energy dissipation and fail to outperform their continuous film counterparts. For γ = 0°, the Offset configurations give rise to aggregated discontinuous sites through the thickness. Therefore, the discontinuous sites function as major defects in the films and lead to little resisted crack opening through the thickness, as illustrated in Figure 16 (a). Therefore, NFC films with DFB architecture at γ = 0° show poor impact resistance. Our results indicate that it might be a good design strategy to disperse fibril ends or defects within films instead of making them aggregated to achieve better impact-resistant films. For γ = 90°, where fibrils align perpendicularly in the thickness direction, the adjacent layers have minimal crack bridging or twisting effects since fibrils in adjacent layers only interact through weak inter-fibril adhesions along the crack opening direction, as shown in Figure 16 (b). By visualizing the simulation trajectory, we only observe significant fibril sliding in the top two layers while localized penetration in other layers. Moreover, we find that the cracks stop propagating in twisted paths, and instead, they grow in vertically straight paths [166, 176]. Therefore, minimal interlayer crack bridging, less fibril sliding, and the lack of crack twisting mechanism collectively lead to the limited energy dissipation capability of the γ = 90° cases.

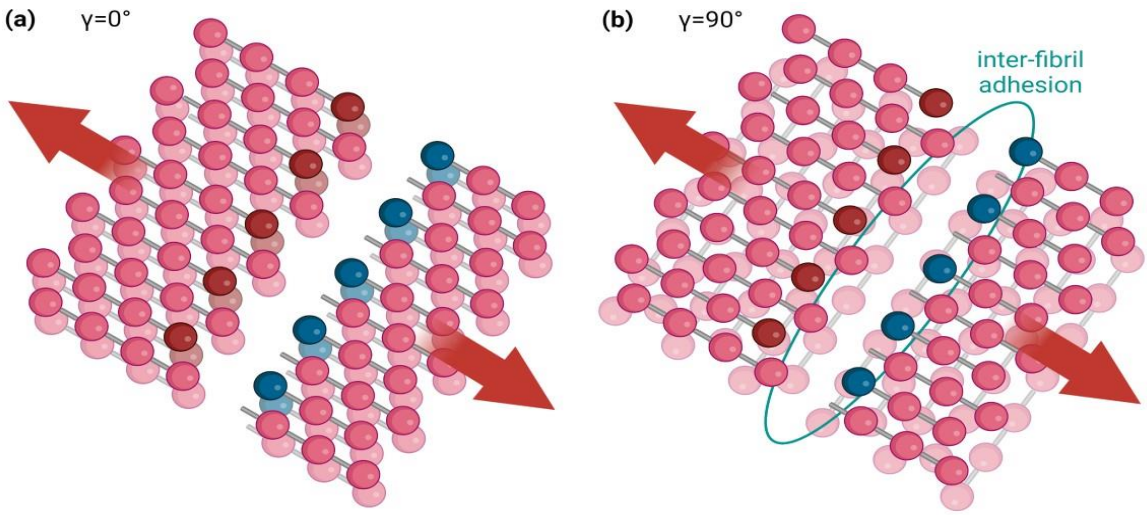

FIGURE 16: Illustrated crack paths. (a) The illustrated crack path for γ = 0° film, where discontinuous sites are at the same location for adjacent layers, leading to little resisted crack opening through the thickness. **(b)** The illustrated crack path for γ = 90° film, where the interlayer crack bridging only comes from weak inter-fibril adhesions along the crack opening direction.

Conversely, we find that NFC films with γ ranging from 18° to 72° utilize a combination of fibril sliding, crack bridging, and crack twisting to enhance their energy dissipation. With increasing γ in this range, we also notice a competition between fibril sliding and crack twisting mechanisms. Specifically, as fibril sliding becomes more significant in a specific layer, more energy is dissipated through this intralayer mechanism. At the same time, through-thickness twisted cracks become less likely to happen, leading to a reduction of energy dissipation in the thickness direction. When $\gamma = 30°$, we see the largest fibril sliding magnitude across the layers (shown in Figure 14(c)), and in the meantime, significant crack twisting is observed across the layers. Therefore, we postulate that the optimal performance in $\gamma = 30°$ is attributed to the fact that it has the most effective combination of fibril sliding, crack bridging, and crack twisting mechanisms.

CHAPTER SIX

SUMMARY

NFC is a promising bio-derived building block to construct impact-resistant films with bioinspired structures. Our study demonstrates that using discontinuous cellulose nanofibrils and adopting specific DFB architecture for the NFC film can outperform the continuously long fibrils in terms of impact resistance against projectile impact.

6.1 Contributions

The specific requirements for the DFB architecture found in this study include achieving critical L and adopting certain configurations that minimize the discontinuous sites (defects) within the impact site as well as applying an optimal γ. We find that the Offset configuration is generally superior to other configurations considered in this study, and the critical L is 750 nm, which is correlated with the size of developed impact propagation zone upon the projectile impact. With L larger than 750 nm, the V_{50}/ρ and $\Delta E_k/\rho$ values start to saturate. We also find that among all the γ considered, $\gamma = 30°$ usually gives rise to the highest V_{50}/ρ and $\Delta E_k/\rho$. By looking into the deformation mechanisms under the projectile impact, we find that the specific DFB architectures utilize a combination of fibril sliding, crack bridging, and crack twisting to enhance their energy dissipation. Also, there seems to exist internal competition between different mechanisms, particularly between fibril sliding and crack twisting. The optimal architectures identified in this study ($L \geq 750$ nm and $\gamma = 30°$) are found to possess the best combination of different mechanisms as shown in Figure 17.

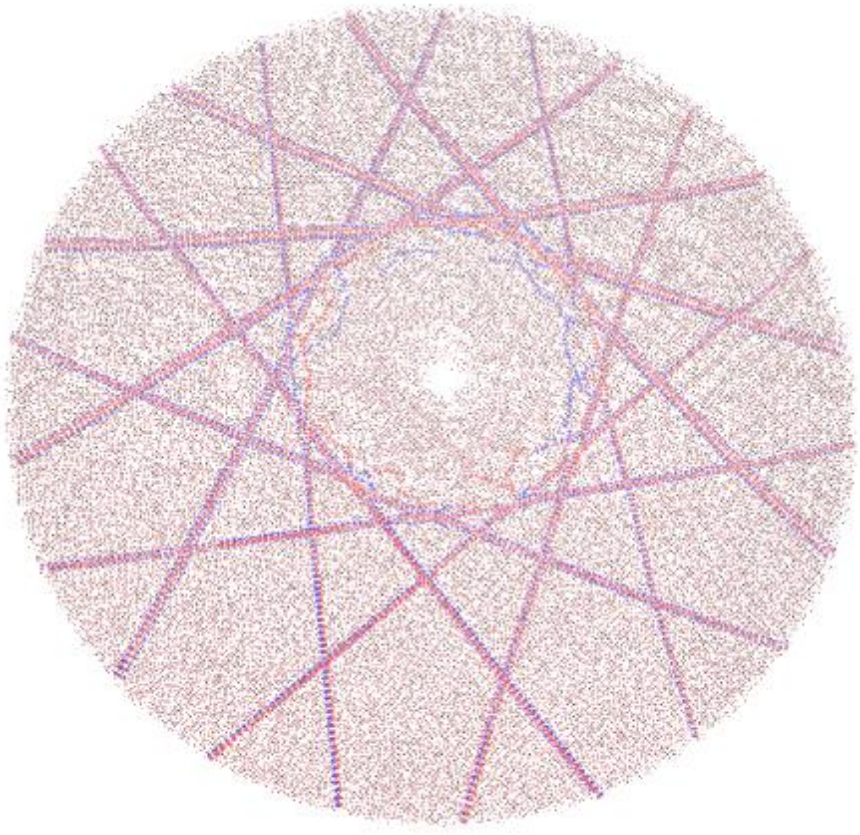

FIGURE 17: Optimized structure for improved impact resistance of Bouligand microstructures with integrated defects.

Overall, we believe our study demonstrates the improved ballistic impact resistance of NFC films with hybrid DFB architecture and unravels the underlying mechanisms. The insights from this study have the potential to guide the future design of protective films made of nanofibrils.

6.2 Future Work

Following this study, we have identified additional work that needs to be done to achieve a comprehensive understanding of the structure-property relationship of NFC films with DFB architecture. First, more simulations with varying projectile sizes and shapes are needed to fully understand how the critical *L* is correlated with the projectile

size and other geometrical factors. We note that theoretical relationships used in our previous studies can be utilized to unravel such size dependences [142, 144, 174]. Second, additional configurations, such as Offset in the thickness direction and Random in both IP and TT, can be considered to see if they offer even better impact resistance against projectile impact. Lastly, it would be interesting to examine other mechanical properties, such as toughness and flexibility, and check whether DFB architecture shows any advantages in improving these properties.

REFERENCES

[1] Moon, R. J., Martini, A., Nairn, J., Simonsen, J., and Youngblood, J., 2011, "Cellulose nanomaterials review: structure, properties and nanocomposites," Chemical Society Reviews, 40(7), 3941-3994.

[2] Sinko, R., Qin, X., and Keten, S., 2015, "Interfacial mechanics of cellulose nanocrystals," Mrs Bulletin, 40(4), 340-348.

[3] Moon, R. J., Schueneman, G. T., and Simonsen, J., 2016, "Overview of cellulose nanomaterials, their capabilities and applications," JOM, 68, 2383-2394.

[4] Morán, J. I., Alvarez, V. A., Cyras, V. P., and Vázquez, A., 2008, "Extraction of cellulose and preparation of nanocellulose from sisal fibers," Cellulose, 15, 149-159.

[5] O'sullivan, A. C., 1997, "Cellulose: the structure slowly unravels," Cellulose, 4, 173-207.

[6] Saito, T., Kimura, S., Nishiyama, Y., and Isogai, A., 2007, "Cellulose nanofibers prepared by TEMPO-mediated oxidation of native cellulose," Biomacromolecules, 8(8), 2485-2491.

[7] Trache, D., Hussin, M. H., Haafiz, M. M., and Thakur, V. K., 2017, "Recent progress in cellulose nanocrystals: sources and production," Nanoscale, 9(5), 1763-1786.

[8] Kargarzadeh, H., Mariano, M., Gopakumar, D., Ahmad, I., Thomas, S., Dufresne, A., Huang, J., and Lin, N., 2018, "Advances in cellulose nanomaterials," Cellulose, 25(4), 2151-2189.

[9] Habibi, Y., 2014, "Key advances in the chemical modification of nanocelluloses," Chem. Soc. Rev., 43(5), 1519-1542.

[10] Elazzouzi-Hafraoui, S., Nishiyama, Y., Putaux, J.-L., Heux, L., Dubreuil, F., and Rochas, C., 2008, "The Shape and Size Distribution of Crystalline Nanoparticles Prepared by Acid Hydrolysis of Native Cellulose," Biomacromolecules, 9(1), 57-65.

[11] Payen, A., 1838, "Mémoire sur la composition du tissu propre des plantes et du ligneux," Comptes rendus, 7(lu 17 décembre 1838), 1052-1056.

[12] Nickerson, R., and Habrle, J., 1947, "Cellulose intercrystalline structure," Industrial & Engineering Chemistry, 39(11), 1507-1512.

[13] Phanthong, P., Reubroycharoen, P., Hao, X., Xu, G., Abudula, A., and Guan, G., 2018, "Nanocellulose: Extraction and application," Carbon Resources Conversion, 1(1), 32-43.

[14] Domingues, R. M., Gomes, M. E., and Reis, R. L., 2014, "The potential of cellulose nanocrystals in tissue engineering strategies," Biomacromolecules, 15(7), 2327-2346.

[15] Beck-Candanedo, S., Roman, M., and Gray, D. G., 2005, "Effect of Reaction Conditions on the Properties and Behavior of Wood Cellulose Nanocrystal Suspensions," Biomacromolecules, 6, 1048.

[16] Araki, J., and Kuga, S., 2001, "Effect of Trace Electrolyte on Liquid Crystal Type of Cellulose Microcrystals," Langmuir, 17, 4493.

[17] De Souza Lima, M. M., Wong, J. T., Paillet, M., Borsali, R., and Pecora, R., 2003, "Translational and rotational dynamics of rodlike cellulose whiskers," Langmuir, 19(1), 24-29.

[18] Araki, J., Wada, M., Kuga, S., and Okano, T., 2000, "Birefringent glassy phase of a cellulose microcrystal suspension," Langmuir, 16(6), 2413-2415.

[19] Dong, X. M., Revol, J.-F., and Gray, D. G., 1998, "Effect of microcrystallite preparation conditions on the formation of colloid crystals of cellulose," Cellulose, 5, 19-32.

[20] Habibi, Y., Goffin, A.-L., Schiltz, N., Duquesne, E., Dubois, P., and Dufresne, A., 2008, "Bionanocomposites based on poly (ε-caprolactone)-grafted cellulose nanocrystals by ring-opening polymerization," Journal of Materials Chemistry, 18(41), 5002-5010.

[21] Dufresne, A., Cavaillé, J. Y., and Helbert, W., 1997, "Thermoplastic nanocomposites filled with wheat straw cellulose whiskers. Part II: effect of processing and modeling," Polymer composites, 18(2), 198-210.
[22] Lu, P., and Hsieh, Y.-L., 2012, "Preparation and characterization of cellulose nanocrystals from rice straw," Carbohydrate Polymers, 87(1), 564-573.
[23] Capadona, J. R., Shanmuganathan, K., Trittschuh, S., Seidel, S., Rowan, S. J., and Weder, C., 2009, "Polymer nanocomposites with nanowhiskers isolated from microcrystalline cellulose," Biomacromolecules, 10(4), 712-716.
[24] Bondeson, D., Mathew, A., and Oksman, K., 2006, "Optimization of the isolation of nanocrystals from microcrystalline cellulose by acid hydrolysis," Cellulose, 13, 171-180.
[25] Hirai, A., Inui, O., Horii, F., and Tsuji, M., 2009, "Phase separation behavior in aqueous suspensions of bacterial cellulose nanocrystals prepared by sulfuric acid treatment," Langmuir, 25(1), 497-502.
[26] Araki, J., Wada, M., Kuga, S., and Okano, T., 1999, "Influence of surface charge on viscosity behavior of cellulose microcrystal suspension," Journal of wood science, 45, 258-261.
[27] Zanoletti, A., Cornelio, A., and Bontempi, E., 2021, "A post-pandemic sustainable scenario: What actions can be pursued to increase the raw materials availability?," Environmental Research, 202, 111681.
[28] Hamad, W., 2006, "On the development and applications of cellulosic nanofibrillar and nanocrystalline materials," The Canadian Journal of Chemical Engineering, 84(5), 513-519.
[29] Dri, F. L., Shang, S., Hector, L. G., Saxe, P., Liu, Z.-K., Moon, R. J., and Zavattieri, P. D., 2014, "Anisotropy and temperature dependence of structural, thermodynamic, and elastic properties of crystalline cellulose Iβ: a first-principles investigation," Modelling and Simulation in Materials Science and Engineering, 22(8), 085012.
[30] Abitbol, T., Rivkin, A., Cao, Y., Nevo, Y., Abraham, E., Ben-Shalom, T., Lapidot, S., and Shoseyov, O., 2016, "Nanocellulose, a tiny fiber with huge applications," Current opinion in biotechnology, 39, 76-88.
[31] Natarajan, B., Emiroglu, C., Obrzut, J., Fox, D. M., Pazmino, B., Douglas, J. F., and Gilman, J. W., 2017, "Dielectric Characterization of Confined Water in Chiral Cellulose Nanocrystal Films," ACS Applied Materials & Interfaces, 9(16), 14222-14231.
[32] Schütz, C., Agthe, M., Fall, A. B., Gordeyeva, K., Guccini, V., Salajková, M., Plivelic, T. S., Lagerwall, J. P. F., Salazar-Alvarez, G., and Bergström, L., 2015, "Rod Packing in Chiral Nematic Cellulose Nanocrystal Dispersions Studied by Small-Angle X-ray Scattering and Laser Diffraction," Langmuir, 31(23), 6507-6513.
[33] Shopsowitz, K. E., Qi, H., Hamad, W. Y., and Maclachlan, M. J., 2010, "Free-standing mesoporous silica films with tunable chiral nematic structures," Nature, 468(7322), 422-425.
[34] Wang, B., and Walther, A., 2015, "Self-Assembled, Iridescent, Crustacean-Mimetic Nanocomposites with Tailored Periodicity and Layered Cuticular Structure," ACS Nano, 9(11), 10637-10646.
[35] Sellinger, A., Weiss, P. M., Nguyen, A., Lu, Y., Assink, R. A., Gong, W., and Brinker, C. J., 1998, "Continuous self-assembly of organic–inorganic nanocomposite coatings that mimic nacre," Nature, 394(6690), 256-260.
[36] Habibi, Y., Lucia, L. A., and Rojas, O. J., 2010, "Cellulose Nanocrystals: Chemistry, Self-Assembly, and Applications," Chemical Reviews, 110(6), 3479-3500.

[37] Xu, X., Liu, F., Jiang, L., Zhu, J. Y., Haagenson, D., and Wiesenborn, D. P., 2013, "Cellulose Nanocrystals vs. Cellulose Nanofibrils: A Comparative Study on Their Microstructures and Effects as Polymer Reinforcing Agents," ACS Applied Materials & Interfaces, 5(8), 2999-3009.
[38] Klemm, D., Kramer, F., Moritz, S., Lindström, T., Ankerfors, M., Gray, D., and Dorris, A., 2011, "Nanocelluloses: a new family of nature‐based materials," Angewandte Chemie International Edition, 50(24), 5438-5466.
[39] Yaradoddi, J. S., Banapurmath, N. R., Ganachari, S. V., Soudagar, M. E. M., Mubarak, N. M., Hallad, S., Hugar, S., and Fayaz, H., 2020, "Biodegradable carboxymethyl cellulose based material for sustainable packaging application," Scientific Reports, 10(1), 21960.
[40] Jeevanandam, J., Rodrigues, J., Pan, S., and Danquah, M. K., 2024, "Chapter 8 - Cellulose-based bionanocomposites: Synthesis, properties, and applications," Advances in Bionanocomposites, Elsevier, 191-210.
[41] Zhu, Y., Hu, J., Luo, H., Young, R. J., Deng, L., Zhang, S., Fan, Y., and Ye, G., 2012, "Rapidly switchable water-sensitive shape-memory cellulose/elastomer nano-composites," Soft Matter, 8, 2509-2517.
[42] Sehaqui, H., Liu, A., Zhou, Q., and Berglund, L. A., 2010, "Fast Preparation Procedure for Large, Flat Cellulose and Cellulose/Inorganic Nanopaper Structures," Biomacromolecules, 11(9), 2195-2198.
[43] Wang, D.-C., Lei, S.-N., Zhong, S., Xiao, X., and Guo, Q.-H., 2023, "Cellulose-Based Conductive Materials for Energy and Sensing Applications," Polymers, 15(20), 4159.
[44] Mtibe, A., Linganiso, L. Z., Mathew, A. P., Oksman, K., John, M. J., and Anandjiwala, R. D., 2015, "A comparative study on properties of micro and nanopapers produced from cellulose and cellulose nanofibres," Carbohydrate Polymers, 118, 1-8.
[45] Pan, J., Hamad, W. Y., and Straus, S. K., 2010, "Parameters Affecting the Chiral Nematic Phase of Nanocrystalline Cellulose Films," Macromolecules, 43(8), 3851-3858.
[46] Reising, A. R., Moon, R., and Youngblood, J., 2012, "Effect of particle alignment on mechanical properties of neat cellulose nanocrystal films," J. Sci. Technol. For. Prod. Processes, 2(6), 32-41.
[47] Wang, B., Torres-Rendon, J. G., Yu, J., Zhang, Y., and Walther, A., 2015, "Aligned bioinspired cellulose nanocrystal-based nanocomposites with synergetic mechanical properties and improved hygromechanical performance," ACS applied materials & interfaces, 7(8), 4595-4607.
[48] Qin, X., Marchi, B. C., Meng, Z., and Keten, S., 2019, "Impact resistance of nanocellulose films with bioinspired Bouligand microstructures," Nanoscale Advances, 1(4), 1351-1361.
[49] Wu, K., Song, Z., Zhang, S., Ni, Y., Cai, S., Gong, X., He, L., and Yu, S.-H., 2020, "Discontinuous fibrous Bouligand architecture enabling formidable fracture resistance with crack orientation insensitivity," Proceedings of the National Academy of Sciences, 117(27), 15465-15472.
[50] Yang W., S. V. R., Gludovatz B., Mackey M., Zimmermann E.A., Chang E.H., Schaible E., Qin Z., Buehler M.J., Ritchie R.O., Meyers M.A, 2014, "Protective role of Arapaima gigas fish scales: Structure and mechanical behavior," Acta Biomaterialia, 10(8), 3599-3614.
[51] Weaver, J. C., Milliron, G. W., Miserez, A., Evans-Lutterodt, K., Herrera, S., Gallana, I., Mershon, W. J., Swanson, B., Zavattieri, P., DiMasi, E., and Kisailus, D., 2012, "The Stomatopod Dactyl Club: A Formidable Damage-Tolerant Biological Hammer," Science, 336(6086), 1275-1280.

[52] Natarajan, B., and Gilman, J. W., 2018, "Bioinspired Bouligand cellulose nanocrystal composites: a review of mechanical properties," Philosophical Transactions of the Royal Society A: Mathematical, Physical and Engineering Sciences, 376(2112), 20170050.
[53] Weaver, J. C., Milliron, G. W., Miserez, A., Evans-Lutterodt, K., Herrera, S., Gallana, I., Mershon, W. J., Swanson, B., Zavattieri, P., DiMasi, E., and Kisailus, D., 2012, "The Stomatopod Dactyl Club: A Formidable Damage-Tolerant Biological Hammer," Science, 336, 1275.
[54] Wang, Y., Zheng, G., Jiang, N., Ying, G., Li, Y., Cai, X., Meng, J., Mai, L., Guo, M., Zhang, Y. S., and Zhang, X., 2023, "Nature-inspired micropatterns," Nature Reviews Methods Primers, 3.
[55] Zhang, X., Parekh, G., Guo, B., Huang, X., Dong, Y., Han, W., Chen, X., and Xiao, G., 2019, "Polyphenol and self-assembly: metal polyphenol nanonetwork for drug delivery and pharmaceutical applications," Future Science, Future Drug Discovery.
[56] Dumanli, A. G., and Savin, T., 2016, "Recent advances in the biomimicry of structural colours," Chemical Society Reviews, 45(24), 6698-6724.
[57] Fratzl, P., 2007, "Biomimetic materials research: what can we really learn from nature's structural materials?," Journal of The Royal Society Interface, 4(15), 637-642.
[58] Hwang, J., Jeong, Y., Park, J. M., Lee, K. H., Hong, J. W., and Choi, J., 2015, "Biomimetics: forecasting the future of science, engineering, and medicine," International journal of nanomedicine, 10(1), 5701-5713.
[59] Egan, P., Sinko, R., Leduc, P. R., and Keten, S., 2015, "The role of mechanics in biological and bio-inspired systems," Nature Communications, 6(1).
[60] Ji, B., and Gao, H., 2010, "Mechanical Principles of Biological Nanocomposites," Annual Review of Materials Research, 40(1), 77-100.
[61] Wegst, U. G. K., Bai, H., Saiz, E., Tomsia, A. P., and Ritchie, R. O., 2015, "Bioinspired structural materials," Nature Materials, 14(1), 23-36.
[62] Aghaei, A., Bochud, N., Rosi, G., and Naili, S., 2021, "Assessing the effective elastic properties of the tendon-to-bone insertion: a multiscale modeling approach," Biomechanics and Modeling in Mechanobiology, 20(2), 433-448.
[63] Chandrasekaran, S., Pankow, M., Peters, K., and Huang, H. Y. S., 2017, "Composition and structure of porcine digital flexor tendon‐bone insertion tissues," Journal of Biomedical Materials Research Part A, 105(11), 3050-3058.
[64] Kannus, P., 2000, "Structure of the tendon connective tissue," Scandinavian Journal of Medicine & Science in Sports, 10(6), 312-320.
[65] Perera, D., Wang, Q., and Schniepp, H. C., 2022, "Multi‐Point Nanoindentation Method to Determine Mechanical Anisotropy in Nanofibrillar Thin Films," Small, 18(30).
[66] Rossetti, L., Kuntz, L. A., Kunold, E., Schock, J., Müller, K. W., Grabmayr, H., Stolberg-Stolberg, J., Pfeiffer, F., Sieber, S. A., Burgkart, R., and Bausch, A. R., 2017, "The microstructure and micromechanics of the tendon–bone insertion," Nature Materials, 16(6), 664-670.
[67] Schwartz, A. G., Pasteris, J. D., Genin, G. M., Daulton, T. L., and Thomopoulos, S., 2012, "Mineral Distributions at the Developing Tendon Enthesis," PLoS ONE, 7(11).
[68] Thomopoulos, S., 2003, "Variation of biomechanical, structural, and compositional properties along the tendon to bone insertion site," Journal of Orthopaedic Research, 21(3), 413-419.
[69] Wang, Y., 2009, "A new algorithm to model the dynamics of 3-D bonded rigid bodies with rotations," Acta Geotechnica, 4(2), 117-127.

[70] Zhang, J., Zhang, H., Wu, T., Wang, Q., and Van Der Spoel, D., 2017, "Comparison of Implicit and Explicit Solvent Models for the Calculation of Solvation Free Energy in Organic Solvents," Journal of Chemical Theory and Computation, 13(3), 1034-1043.
[71] Sang, Z., Xu, L., Ding, R., Wang, M., Yang, X., Li, X., Zhou, B., Gou, K., Han, Y., Liu, T., Chen, X., Cheng, Y., Yang, H., and Li, H., 2023, "Nanoparticles exhibiting virus-mimic surface topology for enhanced oral delivery," Nature Communications, 14(1).
[72] Greenfeld, I., and Wagner, H. D., 2023, "Two natural toughening strategies may inspire sustainable structures," Scientific Reports, 13(1).
[73] Li, Q., Chen, Z., Zhang, Y., Ding, S., Ding, H., Wang, L., Xie, Z., Fu, Y., Wei, M., Liu, S., Chen, J., Wang, X., and Gu, Z., 2023, "Imaging cellular forces with photonic crystals," Nature Communications, 14(1).
[74] Sandak, A., 2023, "Engineered living materials for sustainable and resilient architecture," Nature Reviews Materials, 8(6), 357-359.
[75] An, Y., Yang, Y., Jia, Y., Han, W., and Cheng, Y., 2022, "Mechanical properties of biomimetic ceramic with Bouligand architecture," Journal of the American Ceramic Society, 105(4), 2385-2391.
[76] Jia, Z., Yu, Y., Hou, S., and Wang, L., 2019, "Biomimetic architected materials with improved dynamic performance," Journal of the Mechanics and Physics of Solids, 125, 178-197.
[77] Grunenfelder, L. K. S., N.; Salinas, C.; Milliron, G.; Yaraghi, N.; Herrera, S.; Evans-Lutterodt, K.; Nutt, S.R.; Zavattieri, P.; Kisailus, D., 2014, "Bio-inspired impact-resistant composites," Acta Biomaterialia, 10(9), 3997-4008.
[78] Islam, M. K., Hazell, P. J., Escobedo, J. P., and Wang, H., 2021, "Biomimetic armour design strategies for additive manufacturing: A review," Materials & Design, 205.
[79] Schleper, A., 2020, "Impact Resistant 3-D Printed Structures," The Journal of Undergraduate Research, 17(1).
[80] An, Y., Song, M., Wan, K., Jia, Y., Yang, Y., and Cheng, Y., 2023, "Anisotropic friction properties of biomimetic Cf/ZrB2-SiC ceramic composites with bouligand structures," Tribology International, 186(8).
[81] Chen, Y., Dang, B., Fu, J., Zhang, J., Liang, H., Sun, Q., Zhai, T., and Li, H., 2022, "Bioinspired Construction of Micronano Lignocellulose into an Impact Resistance “Wooden Armor” With Bouligand Structure," ACS Nano, 16(5), 7525-7534.
[82] Barthelat, F., Tang, H., Zavattieri, P., Li, C.-M., and Espinosa, H., 2007, "On the mechanics of mother-of-pearl: a key feature in the material hierarchical structure," Journal of the Mechanics and Physics of Solids, 55(2), 306-337.
[83] Barthelat, F., Yin, Z., and Buehler, M. J., 2016, "Structure and mechanics of interfaces in biological materials," Nature Reviews Materials, 1(4), 1-16.
[84] Espinosa, H. D., Rim, J. E., Barthelat, F., and Buehler, M. J., 2009, "Merger of structure and material in nacre and bone–Perspectives on de novo biomimetic materials," Progress in Materials Science, 54(8), 1059-1100.
[85] Yin, Z., Hannard, F., and Barthelat, F., 2019, "Impact-resistant nacre-like transparent materials," Science, 364(6447), 1260-1263.
[86] Gao, H., Ji, B., Jäger, I. L., Arzt, E., and Fratzl, P., 2003, "Materials become insensitive to flaws at nanoscale: Lessons from nature," Proceedings of the National Academy of Sciences, 100(10), 5597-5600.

[87] Li, X., Chang, W.-C., Chao, Y. J., Wang, R., and Chang, M., 2004, "Nanoscale Structural and Mechanical Characterization of a Natural Nanocomposite Material: The Shell of Red Abalone," Nano Letters, 4(4), 613-617.
[88] Guarín-Zapata, N., Gomez, J., Yaraghi, N., Kisailus, D., and Zavattieri, P. D., 2015, "Shear wave filtering in naturally-occurring Bouligand structures," Acta Biomaterialia, 23, 11-20.
[89] Lee, J. H., Loya, P. E., Lou, J., and Thomas, E. L., 2014, "Dynamic mechanical behavior of multilayer graphene via supersonic projectile penetration," Science, 346(6213), 1092-1096.
[90] Lee, J.-H., Veysset, D., Singer, J. P., Retsch, M., Saini, G., Pezeril, T., Nelson, K. A., and Thomas, E. L., 2012, "High strain rate deformation of layered nanocomposites," Nature Communications, 3(11).
[91] Marchi, B. C., and Keten, S., 2019, "Microstructure and size effects on the mechanics of two dimensional, high aspect ratio nanoparticle assemblies," Frontiers in Materials, 6(174).
[92] Mencattelli, L., and Pinho, S. T., 2020, "Ultra-thin-ply CFRP Bouligand bio-inspired structures with enhanced load-bearing capacity, delayed catastrophic failure and high energy dissipation capability," Composites Part A: Applied Science and Manufacturing, 129(105655).
[93] Raabe, D., Romano, P., Sachs, C., Fabritius, H., Al-Sawalmih, A., Yi, S.-B., Servos, G., and Hartwig, H., 2006, "Microstructure and crystallographic texture of the chitin–protein network in the biological composite material of the exoskeleton of the lobster Homarus americanus," Materials science and engineering: A, 421(1-2), 143-153.
[94] Hild, S., Neues, F., Žnidaršič, N., Štrus, J., Epple, M., Marti, O., and Ziegler, A., 2009, "Ultrastructure and mineral distribution in the tergal cuticle of the terrestrial isopod Titanethes albus. Adaptations to a karst cave biotope," Journal of Structural Biology, 168(3), 426-436.
[95] Fabritius, H. O., Sachs, C., Triguero, P. R., and Raabe, D., 2009, "Influence of structural principles on the mechanics of a biological fiber ‐ based composite material with hierarchical organization: the exoskeleton of the lobster Homarus americanus," Advanced materials, 21(4), 391-400.
[96] Seidl, B., Huemer, K., Neues, F., Hild, S., Epple, M., and Ziegler, A., 2011, "Ultrastructure and mineral distribution in the tergite cuticle of the beach isopod Tylos europaeus Arcangeli, 1938," Journal of structural biology, 174(3), 512-526.
[97] Seidl, B. H., and Ziegler, A., 2012, "Electron microscopic and preparative methods for the analysis of isopod cuticle," ZooKeys(176), 73.
[98] Ruangchai, S., Reisecker, C., Hild, S., and Ziegler, A., 2013, "The architecture of the joint head cuticle and its transition to the arthrodial membrane in the terrestrial crustacean Porcellio scaber," Journal of structural biology, 182(1), 22-35.
[99] Alagboso, F. I., Reisecker, C., Hild, S., and Ziegler, A., 2014, "Ultrastructure and mineral composition of the cornea cuticle in the compound eyes of a supralittoral and a marine isopod," Journal of Structural Biology, 187(2), 158-173.
[100] Huber, J., Fabritius, H.-O., Griesshaber, E., and Ziegler, A., 2014, "Function-related adaptations of ultrastructure, mineral phase distribution and mechanical properties in the incisive cuticle of mandibles of Porcellio scaber Latreille, 1804," Journal of structural biology, 188(1), 1-15.
[101] Huber, J., Griesshaber, E., Nindiyasari, F., Schmahl, W. W., and Ziegler, A., 2015, "Functionalization of biomineral reinforcement in crustacean cuticle: calcite orientation in the partes incisivae of the mandibles of Porcellio scaber and the supralittoral species Tylos europaeus (Oniscidea, Isopoda)," Journal of Structural Biology, 190(2), 173-191.

[102] Fabritius, H.-O., Ziegler, A., Friák, M., Nikolov, S., Huber, J., Seidl, B. H. M., Ruangchai, S., Alagboso, F. I., Karsten, S., Lu, J., Janus, A. M., Petrov, M., Zhu, L.-F., Hemzalová, P., Hild, S., Raabe, D., and Neugebauer, J., 2016, "Functional adaptation of crustacean exoskeletal elements through structural and compositional diversity: a combined experimental and theoretical study," Bioinspiration & Biomimetics, 11(5), 055006.
[103] Li, S., Bai, H., Shepherd, R. F., and Zhao, H., 2019, "Bio‐inspired Design and Additive Manufacturing of Soft Materials, Machines, Robots, and Haptic Interfaces," Angewandte Chemie International Edition, 58(33), 11182-11204.
[104] Liu, K., Tang, S., Zhu, L., Wen, W., Liu, M., Li, H., Zhou, C., and Luo, B., 2022, "Bio-Inspired Liquid Crystal Gel with Adjustable Viscoelasticity to Modulate Cell Behaviors and Fate," Composites, Part B, 234, 109704.
[105] Liu, P., Wang, J., Qi, H., Koddenberg, T., Xu, D., Liu, S., and Zhang, K., 2022, "Biomimetic Confined Self-Assembly of Chitin Nanocrystals," Nano Today, 43, 101420.
[106] Luo, Y., Li, Y., Liu, K., Li, L., Wen, W., Ding, S., Huang, Y., Liu, M., Zhou, C., and Luo, B., 2023, "Modulating of Bouligand Structure and Chirality Constructed Bionically Based on the Self-Assembly of Chitin Whiskers," Biomacromolecules.
[107] Mencattelli, L., and Pinho, S., 2019, "Realising bio-inspired impact damage-tolerant thin-ply CFRP Bouligand structures via promoting diffused sub-critical helicoidal damage," Composites Science and Technology, 107684.
[108] Meo, M., Rizzo, F., Portus, M., and Pinto, F., 2021, "Bioinspired Helicoidal Composite Structure Featuring Functionally Graded Variable Ply Pitch," Materials, 14(18), 5133.
[109] Mohammadi, P., Toivonen, M. S., Ikkala, O., Wagermaier, W., and Linder, M. B., 2017, "Aligning cellulose nanofibril dispersions for tougher fibers," Scientific Reports, 7(1).
[110] Narkevicius, A., Parker, R. M., Ferrer-Orri, J., Parton, T. G., Lu, Z. H., van de Kerkhof, G. T., Frka-Petesic, B., and Vignolini, S., 2022, "Revealing the Structural Coloration of Self-Assembled Chitin Nanocrystal Films," Adv. Mater., 34, 2203300.
[111] Narkevicius, A., Steiner, L. M., Parker, R. M., Ogawa, Y., Frka-Petesic, B., and Vignolini, S., 2019, "Controlling the Self-Assembly Behavior of Aqueous Chitin Nanocrystal Suspensions," Biomacromolecules, 20, 2830.
[112] Phoenix, S. L., and Raj, R., 1992, "Overview no. 100 Scalings in fracture probabilities for a brittle matrix fiber composite," Acta Metallurgica et Materialia, 40(11), 2813-2828.
[113] Shishehbor, M., Son, H., Nuruddin, M., Youngblood, J. P., Davis, C., and Zavattieri, P. D., 2021, "Influence of alignment and microstructure features on the mechanical properties and failure mechanisms of cellulose nanocrystals (CNC) films," Journal of the Mechanical Behavior of Biomedical Materials, 118, 104399.
[114] Yang, F., and Xie, W., 2022, "Thermal buckling behavior of Bouligand inspired laminated composite plates," Journal of Composite Materials, 56(26), 3939-3947.
[115] Jia, Z., Yu, Y., and Wang, L., 2019, "Learning from nature: Use material architecture to break the performance tradeoffs," Materials & Design, 168, 107650.
[116] Jia, Z., and Wang, L., 2019, "3D printing of biomimetic composites with improved fracture toughness," Acta Materialia, 173, 61-73.
[117] Torres, A. M., Trikanad, A. A., Aubin, C. A., Lambers, F. M., Luna, M., Rimnac, C. M., Zavattieri, P., and Hernandez, C. J., 2019, "Bone-inspired microarchitectures achieve enhanced fatigue life," Proceedings of the National Academy of Sciences, 116(49), 24457-24462.

[118] Jackson, A., Vincent, J. F., and Turner, R., 1988, "The mechanical design of nacre," Proceedings of the Royal society of London. Series B. Biological sciences, 234(1277), 415-440.
[119] Shang, J., Ngern, N. H., and Tan, V. B., 2016, "Crustacean-inspired helicoidal laminates," Composites Science and Technology, 128, 222-232.
[120] Ginzburg, D., Pinto, F., Iervolino, O., and Meo, M., 2017, "Damage tolerance of bio-inspired helicoidal composites under low velocity impact," Composite Structures, 161, 187-203.
[121] Kose, O., Tran, A., Lewis, L., Hamad, W. Y., and MacLachlan, M. J., 2019, "Unwinding a Spiral of Cellulose Nanocrystals for Stimuli-Responsive Stretchable Optics," Nat. Commun., 10, 510.
[122] Kádár, R., Spirk, S., and Nypelo, T., 2021, "Cellulose Nanocrystal Liquid Crystal Phases: Progress and Challenges in Characterization Using Rheology Coupled to Optics, Scattering, and Spectroscopy," ACS Nano, 15, 7931.
[123] Saffarionpour, S., 2020, "Nanocellulose for Stabilization of Pickering Emulsions and Delivery of Nutraceuticals and Its Interfacial Adsorption Mechanism," Food and Bioprocess Technology, 13.
[124] Fleming, K., Gray, D. G., and Matthews, S., 2001, "Cellulose crystallites," Chemistry–A European Journal, 7(9), 1831-1836.
[125] Luo, Y., Li, Y., Liu, K., Li, L., Wen, W., Ding, S., Huang, Y., Liu, M., Zhou, C., and Luo, B., 2023, "Modulating of Bouligand Structure and Chirality Constructed Bionically Based on the Self-Assembly of Chitin Whiskers," Biomacromolecules, 24(6), 2942-2954.
[126] Chami Khazraji, A., and Robert, S., 2013, "Self-Assembly and Intermolecular Forces When Cellulose and Water Interact Using Molecular Modeling," Journal of Nanomaterials, 2013, 1-12.
[127] Parker, R. M., Frka-Petesic, B., Guidetti, G., Kamita, G., Consani, G., Abell, C., and Vignolini, S., 2016, "Hierarchical Self-Assembly of Cellulose Nanocrystals in a Confined Geometry," ACS Nano, 10, 8443.
[128] Parton, T. G., Parker, R. M., Van De Kerkhof, G. T., Narkevicius, A., Haataja, J. S., Frka-Petesic, B., and Vignolini, S., 2022, "Chiral self-assembly of cellulose nanocrystals is driven by crystallite bundles," Nature Communications, 13(1).
[129] Youngblood, J. P., and Sottos, N. R., 2008, "Bioinspired Materials for Self-Cleaning and Self-Healing," MRS Bulletin, 33(8), 732-741.
[130] Parker, R. M., Guidetti, G., Williams, C. A., Zhao, T., Narkevicius, A., Vignolini, S., and Frka-Petesic, B., 2018, "The Self-Assembly of Cellulose Nanocrystals: Hierarchical Design of Visual Appearance," Advanced Materials, 30(19), 1704477.
[131] Mencattelli, L., and Pinho, S. T., 2020, "Herringbone-Bouligand CFRP structures: A new tailorable damage-tolerant solution for damage containment and reduced delaminations," Composites Science and Technology, 190, 108047.
[132] Quan, H., Yang, W., Schaible, E., Ritchie, R. O., and Meyers, M. A., 2018, "Novel Defense Mechanisms in the Armor of the Scales of the “Living Fossil” Coelacanth Fish," Advanced Functional Materials, 28(46), 1804237.
[133] Yin, S., Yang, W., Kwon, J., Wat, A., Meyers, M. A., and Ritchie, R. O., 2019, "Hyperelastic phase-field fracture mechanics modeling of the toughening induced by Bouligand structures in natural materials," Journal of the Mechanics and Physics of Solids, 131, 204-220.
[134] Nikolov, S., Petrov, M., Lymperakis, L., Friák, M., Sachs, C., Fabritius, H.-O., Raabe, D., and Neugebauer, J., 2010, "Revealing the Design Principles of High-Performance Biological

Composites Using Ab initio and Multiscale Simulations: The Example of Lobster Cuticle," Advanced Materials, 22(4), 519-526.
[135] Yeo, J., Jung, G., Tarakanova, A., Martín-Martínez, F. J., Qin, Z., Cheng, Y., Zhang, Y.-W., and Buehler, M. J., 2018, "Multiscale modeling of keratin, collagen, elastin and related human diseases: Perspectives from atomistic to coarse-grained molecular dynamics simulations," Extreme Mechanics Letters, 20, 112-124.
[136] Hsu, D. D., Xia, W., Arturo, S. G., and Keten, S., 2014, "Systematic Method for Thermomechanically Consistent Coarse-Graining: A Universal Model for Methacrylate-Based Polymers," Journal of Chemical Theory and Computation, 10(6), 2514-2527.
[137] Noid, W. G., 2013, "Perspective: Coarse-grained models for biomolecular systems," The Journal of Chemical Physics, 139(9), 090901.
[138] Ruiz, L., Xia, W., Meng, Z., and Keten, S., 2015, "A coarse-grained model for the mechanical behavior of multi-layer graphene," Carbon, 82, 103-115.
[139] Caviness, C., Chen, Y., Yang, Z., Wang, H., Wu, Y., and Meng, Z., 2023, "Improved Ballistic Impact Resistance of Nanofibrillar Cellulose Films With Discontinuous Fibrous Bouligand Architecture," Journal of Applied Mechanics, 91, 1-24.
[140] Meng, Q., Gao, Y., Shi, X., and Feng, X.-Q., 2022, "Three-dimensional crack bridging model of biological materials with twisted Bouligand structures," Journal of the Mechanics and Physics of Solids, 159, 104729.
[141] Meng, Z., Bessa, M. A., Xia, W., Kam Liu, W., and Keten, S., 2016, "Predicting the Macroscopic Fracture Energy of Epoxy Resins from Atomistic Molecular Simulations," Macromolecules, 49(24), 9474-9483.
[142] Meng, Z., and Keten, S., 2018, "Unraveling the Effect of Material Properties and Geometrical Factors on Ballistic Penetration Energy of Nanoscale Thin Films," Journal of Applied Mechanics, 85(12).
[143] Meng, Z., Singh, A., Qin, X., and Keten, S., 2017, "Reduced ballistic limit velocity of graphene membranes due to cone wave reflection," Extreme Mechanics Letters, 15, 70-77.
[144] Qin, X., Feng, S., Meng, Z., and Keten, S., 2017, "Optimizing the mechanical properties of cellulose nanopaper through surface energy and critical length scale considerations," Cellulose, 24(8), 3289-3299.
[145] Yang, Z., Chiang, C.-C., and Meng, Z., 2023, "Investigation of dynamic impact responses of layered polymer-graphene nanocomposite films using coarse-grained molecular dynamics simulations," Carbon, 203, 202-210.
[146] Ramezani, M. G., and Golchinfar, B., 2019, "Mechanical properties of cellulose nanocrystal (cnc) bundles: Coarse-grained molecular dynamic simulation," Journal of Composites Science, 3(2), 57.
[147] Shishehbor, M., and Zavattieri, P. D., 2019, "Effects of interface properties on the mechanical properties of bio-inspired cellulose nanocrystal (CNC)-based materials," Journal of the Mechanics and Physics of Solids, 124, 871-896.
[148] Mehandzhiyski, A. Y., Rolland, N., Garg, M., Wohlert, J., Linares, M., and Zozoulenko, I., 2020, "A novel supra coarse-grained model for cellulose," Cellulose, 27, 4221-4234.
[149] Rolland, N., Mehandzhiyski, A. Y., Garg, M., Linares, M., and Zozoulenko, I. V., 2020, "New patchy particle model with anisotropic patches for molecular dynamics simulations: Application to a coarse-grained model of cellulose Nanocrystal," Journal of chemical theory and computation, 16(6), 3699-3711.

[150] Wu, Z., Beltran-Villegas, D. J., and Jayaraman, A., 2020, "Development of a new coarse-grained model to simulate assembly of cellulose chains due to hydrogen bonding," Journal of Chemical Theory and Computation, 16(7), 4599-4614.
[151] Ray, U., Pang, Z., and Li, T., 2021, "Mechanics of cellulose nanopaper using a scalable coarse-grained modeling scheme," Cellulose, 28, 3359-3372.
[152] Phoenix, S., Ibnabdeljalil, M., and Hui, C.-Y., 1997, "Size effects in the distribution for strength of brittle matrix fibrous composites," International Journal of Solids and Structures, 34(5), 545-568.
[153] Menig, R., Meyers, M., Meyers, M., and Vecchio, K., 2000, "Quasi-static and dynamic mechanical response of Haliotis rufescens (abalone) shells," Acta materialia, 48(9), 2383-2398.
[154] Chen, B., Wu, P., and Gao, H., 2009, "A characteristic length for stress transfer in the nanostructure of biological composites," Composites Science and Technology, 69(7-8), 1160-1164.
[155] Landis, C. M., McGlockton, M. A., and McMeeking, R. M., 1999, "An Improved Shear Lag Model for Broken Fibers in Composite Materials," Journal of Composite Materials, 33(7), 667-680.
[156] Wei, X., Filleter, T., and Espinosa, H. D., 2015, "Statistical shear lag model–Unraveling the size effect in hierarchical composites," Acta biomaterialia, 18, 206-212.
[157] Daniels, H. E., 1945, "The statistical theory of the strength of bundles of threads. I," Proceedings of the Royal Society of London. Series A. Mathematical and Physical Sciences, 183(995), 405-435.
[158] Tang, H., Barthelat, F., and Espinosa, H., 2007, "An elasto-viscoplastic interface model for investigating the constitutive behavior of nacre," Journal of the Mechanics and Physics of Solids, 55(7), 1410-1438.
[159] Harley, R., James, D., Miller, A., and White, J., 1977, "Phonons and the elastic moduli of collagen and muscle," Nature, 267(5608), 285-287.
[160] Keten, S., Xu, Z., Ihle, B., and Buehler, M. J., 2010, "Nanoconfinement controls stiffness, strength and mechanical toughness of β-sheet crystals in silk," Nature Materials, 9(4), 359-367.
[161] Gao, X. L., and Li, K., 2005, "A shear-lag model for carbon nanotube-reinforced polymer composites," International Journal of Solids and Structures, 42(5), 1649-1667.
[162] Kimura, F., Kimura, T., Tamura, M., Hirai, A., Ikuno, M., and Horii, F., 2005, "Magnetic alignment of the chiral nematic phase of a cellulose microfibril suspension," Langmuir, 21(5), 2034-2037.
[163] George, J., and S N, S., 2015, "Cellulose nanocrystals: synthesis, functional properties, and applications," Nanotechnology, Science and Applications, 45.
[164] Yaraghi, N. A., Guarín‐Zapata, N., Grunenfelder, L. K., Hintsala, E., Bhowmick, S., Hiller, J. M., Betts, M., Principe, E. L., Jung, J. Y., Sheppard, L., Wuhrer, R., McKittrick, J., Zavattieri, P. D., and Kisailus, D., 2016, "A Sinusoidally Architected Helicoidal Biocomposite," Advanced Materials, 28(32), 6835-6844.
[165] Yaraghi, N. A., Trikanad, A. A., Restrepo, D., Huang, W., Rivera, J., Herrera, S., Zhernenkov, M., Parkinson, D. Y., Caldwell, R. L., Zavattieri, P. D., and Kisailus, D., 2019, "The Stomatopod Telson: Convergent Evolution in the Development of a Biological Shield," Advanced Functional Materials, 29(34), 1902238.

[166] Suksangpanya, N., Yaraghi, N. A., Pipes, R. B., Kisailus, D., and Zavattieri, P., 2018, "Crack twisting and toughening strategies in Bouligand architectures," International Journal of Solids and Structures, 150, 83-106.
[167] Song, Z., Ni, Y., and Cai, S., 2019, "Fracture modes and hybrid toughening mechanisms in oscillated/twisted plywood structure," Acta biomaterialia, 91, 284-293.
[168] Amini, S., Tadayon, M., Idapalapati, S., and Miserez, A., 2015, "The role of quasi-plasticity in the extreme contact damage tolerance of the stomatopod dactyl club," Nature materials, 14(9), 943-950.
[169] Yang, W., Quan, H., Meyers, M. A., and Ritchie, R. O., 2019, "Arapaima fish scale: One of the toughest flexible biological materials," Matter, 1(6), 1557-1566.
[170] Plimpton, S., 1995, "Fast Parallel Algorithms for Short-Range Molecular Dynamics," Journal of Computational Physics, 117(1), 1-19.
[171] Humphrey, W. D., A.; Schulten, K., 1996, "VMD: Visual Molecular Dynamics," Journal of Molecular Graphics, 14(1), 6.
[172] Wu, X., Moon, R. J., and Martini, A., 2014, "Tensile strength of I β crystalline cellulose predicted by molecular dynamics simulation," Cellulose, 21, 2233-2245.
[173] Hazzard, M. K., Hallett, S., Curtis, P. T., Iannucci, L., and Trask, R. S., 2017, "Effect of fibre orientation on the low velocity impact response of thin Dyneema® composite laminates," International Journal of Impact Engineering, 100, 35-45.
[174] Xia, W., Ruiz, L., Pugno, N. M., and Keten, S., 2016, "Critical length scales and strain localization govern the mechanical performance of multi-layer graphene assemblies," Nanoscale, 8(12), 6456-6462.
[175] Ritchie, R. O., 2011, "The conflicts between strength and toughness," Nature materials, 10(11), 817-822.
[176] Suksangpanya, N., Yaraghi, N. A., Kisailus, D., and Zavattieri, P., 2017, "Twisting cracks in Bouligand structures," Journal of the mechanical behavior of biomedical materials, 76, 38-57.
[177] Alwan, F. H. A., Prabowo, A. R., Muttaqie, T., Muhayat, N., Ridwan, R., and Laksono, F. B., 2022, "Assessment of ballistic impact damage on aluminum and magnesium alloys against high velocity bullets by dynamic FE simulations," Journal of the Mechanical Behavior of Materials, 31(1), 595-616.
[178] Ouyang, W., Gong, B., Wang, H., Scarpa, F., Su, B., and Peng, H.-X., 2021, "Identifying optimal rotating pitch angles in composites with Bouligand structure," Composites Communications, 23, 100602.
[179] Tabiei, A., and Nilakantan, G., 2008, "Ballistic Impact of Dry Woven Fabric Composites: A Review," Applied Mechanics Reviews, 61(1).